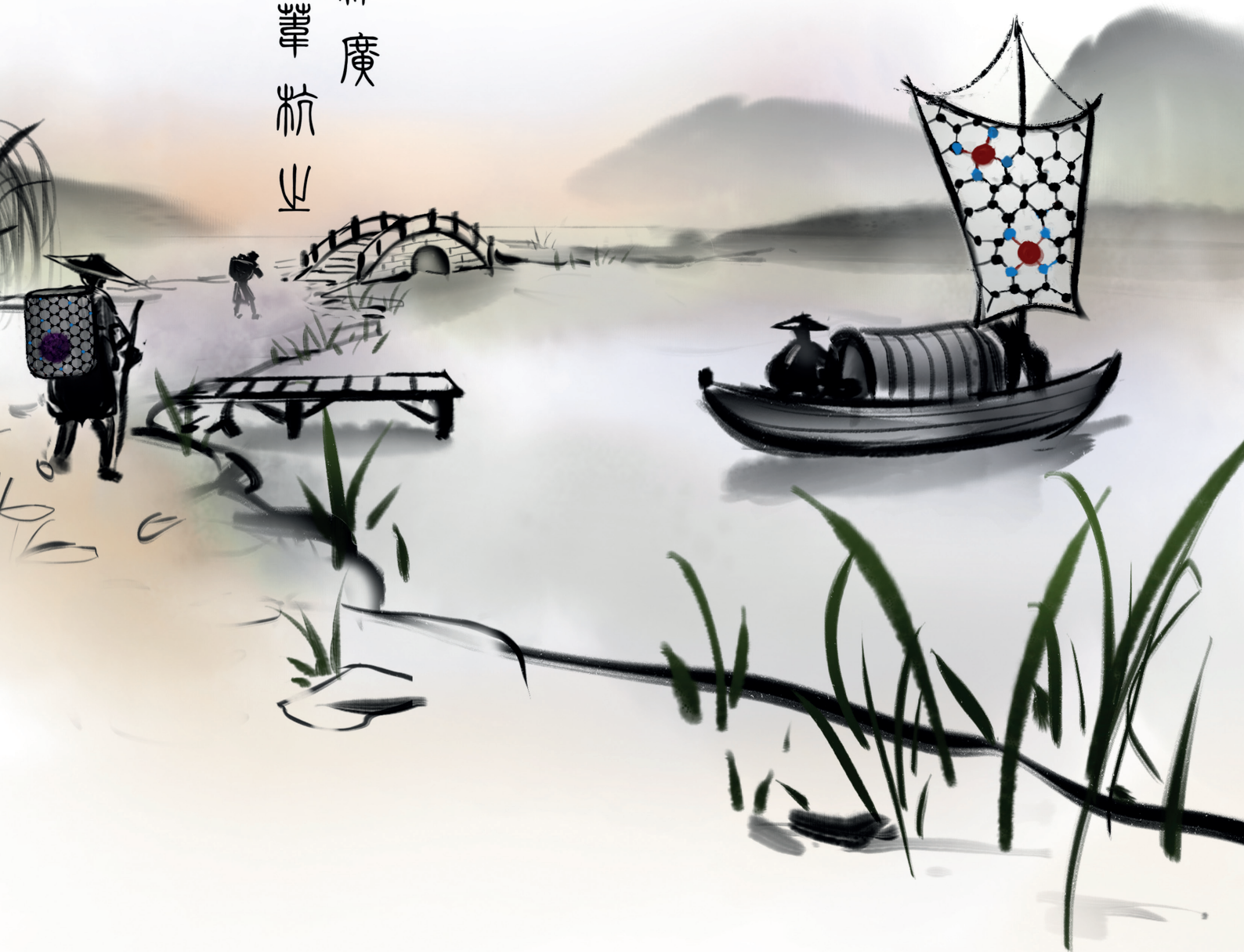


ADVANCED MATERIALS



誰
謂
一
華
杭
山



Carbon-Supported Single Atom Catalysts for Electrochemical Energy Conversion and Storage

Yi Peng, Bingzhang Lu, and Shaowei Chen*

In celebration of the 60th Anniversary of the University of Science and Technology of China

Single atoms of select transition metals supported on carbon substrates have emerged as a unique system for electrocatalysis because of maximal atom utilization ($\approx 100\%$) and high efficiency for a range of reactions involved in electrochemical energy conversion and storage, such as the oxygen reduction, oxygen evolution, hydrogen evolution, and CO_2 reduction reactions. Herein, the leading strategies for the preparation of single atom catalysts are summarized, and the electrocatalytic performance of the resulting samples for the various reactions is discussed. In general, the carbon substrate not only provides a stabilizing matrix for the metal atoms, but also impacts the electronic density of the metal atoms due to strong interfacial interactions, which may lead to the formation of additional active sites by the adjacent carbon atoms and hence enhanced electrocatalytic activity. This necessitates a detailed understanding of the material structures at the atomic level, a critical step in the construction of a relevant structural model for theoretical simulations and calculations. Finally, a perspective is included highlighting the promises and challenges for the future development of carbon-supported single atom catalysts in electrocatalysis.

1. Introduction

Transition-metal nanoparticles, such as Ru, Rh, Pd, Ag, Ir, Pt, and Au, have been used extensively as effective catalysts in a wide range of electrochemical reactions for energy conversion and storage, such as hydrogen evolution reaction (HER), oxygen reduction reaction (ORR), oxygen evolution reaction (OER), and carbon dioxide reduction reaction (CO_2RR).^[1–9] However, the high costs and/or low natural abundance of noble metals significantly hamper the wide-spread applications of these technologies. One way to mitigate these issues is to minimize the usage of these materials without compromising the catalytic performance, thus leading to drastic enhancement of the specific/mass activity. Toward this end, a variety of strategies have been developed, which have been primarily focused on structural manipulation of the metal nanoparticles within the context of core size,^[10–13] shape,^[14–17] crystalline facets,^[18–23]

alloying with other noble or non-noble metals,^[24–28] and hybridization of noble metal catalysts with other materials.^[29–35]


As the reactions take place only on the nanoparticle catalyst surface and the adsorption of reactants and desorption of products at the active sites represent key steps that largely dictate the catalytic efficiency, the reaction dynamics has been found to be readily manipulated by nanoparticle size and shape, and the catalytic activity is mostly dominated by the surface atoms with minimal contributions from the inner core. Recent research has shown that shrinking of the nanoparticle size down to the sub-nanometer regime leads to an increasing number of under-coordinated metal atoms that may serve as catalytic active sites, which will reach a maximum at the single atom level when individual metal atoms are accessible and catalytically active.^[36] Furthermore, to enhance dispersion and stability, nano-

particle catalysts are generally supported on a substrate surface, and the metal-substrate electronic interactions have long been recognized to play an important role in manipulating the electronic structure of the metal nanoparticles and hence interactions with reaction intermediates.^[37] This has indeed been exploited as a unique variable in the mechanistic control of nanoparticle catalytic performance. It can be envisaged that when the nanoparticle size diminishes to the single atom level, such metal-substrate interactions will be maximized, which may lead to the generation of new catalytic active sites, emergence of new reaction pathways, and eventually enhancement of the catalytic performance.^[38,39] Because of these, single atom catalysis has been attracting a great deal of attention lately.

It should be noted that for decades a wide variety of organometallic complexes have been used as effective catalysts in diverse electrocatalytic reactions.^[40] As they generally contain individual metal centers, one may argue that these compounds represent the early examples of single atom catalysts (SACs). Thus far, there has been no clear, strict definition of SACs, which typically refer to single metal atoms embedded within a solid matrix, such as a metal, metal oxide, metal nitride, or carbon, and the resulting nanostructures behave as heterogeneous catalysts, in contrast to organometallic compounds that are typically involved in homogeneous catalysis.^[41]

Back in 1991, the Basset group reported the first preparation of SACs based on silica-supported zirconium and tantalum

Y. Peng, B. Z. Lu, Prof. S. W. Chen
Department of Chemistry and Biochemistry
University of California
1156 High Street, Santa Cruz, CA 95064, USA
E-mail: shaowei@ucsc.edu

 The ORCID identification number(s) for the author(s) of this article can be found under <https://doi.org/10.1002/adma.201801995>.

DOI: 10.1002/adma.201801995

complexes and their applications in heterogeneous catalysis.^[42,43] In 2011, Zhang and coworkers deposited single Pt atoms supported on iron oxide for CO oxidation.^[44] Both experimental studies and density functional theory (DFT) calculations showed that the high catalytic activity was due to the partially vacant 5d orbitals of the high-valence, positively charged Pt atoms which lowered the CO adsorption energy and activation barrier for CO oxidation. This is in sharp contrast with bulk Pt surfaces that are known to be readily poisoned by CO due to strong adsorption of CO. Subsequently, a range of SACs (e.g., Ir, Pt, Au, Rh, and Pd) have been prepared on various substrates such as TiN, Al₂O₃, TiO₂, ZnO, Co₃O₄, FeO_x, and CeO₂,^[45–64] and shown apparent catalytic activity toward diverse reactions such as hydrogenation, CO oxidation, and water gas-shift reaction, as summarized in several recent review articles.^[36,65–68]

In recent years, SACs have also found significant applications in electrochemical energy conversion and storage, in particular, ORR, OER, HER, and CO₂RR,^[69–111] and the results suggest that the supporting substrates such as carbon-based materials not only provide anchoring sites for the single metal atoms, offer good electrical conductance with the graphitic skeletons, but also manipulate the charge density and electronic structure of the metal atoms because of strong interfacial interactions between the metal atoms and adjacent carbon atoms. Such attributes may be exploited for the enhancement of the electrocatalytic performance due to generation of an increasing number of active sites.

Toward this end, DFT is a powerful tool to probe the geometric configuration and electronic structure of SACs, a critical step in unraveling the mechanistic insights into the reaction dynamics.^[112] Specifically, DFT calculations may yield quantitative information of the bond length, bond angle, charge density distribution, and Bader charge that are critical in examining the binding energy of reaction intermediates to the metal atoms.^[77,109] The resulting density of states (DOS) can be used to identify whether the system is metallic or insulating, and the extent of electron delocalization of the metal atoms.^[113] By analyzing the DOS at the Fermi level, one can identify the specific atoms that make contributions to the states, which play a significant role in determining the chemical reaction dynamics.^[114] Moreover, free energy of elementary reaction steps can be quantitatively estimated by calculating the binding energy, entropy, zero-point energy and solvation energy of possible intermediates on the catalyst. From the resulting energy diagram, one can identify rate determine steps and compare the activity among various atomic sites, an effective procedure in the identification of catalytic active sites.^[115–117]

In this review, we will first summarize leading methods used in the preparation of SACs supported on carbon-based materials, and then highlight their unique electrocatalytic activity toward important reactions in electrochemical energy conversions and storages, such as HER, ORR, OER, and CO₂RR. The roles and contributions of the metal atoms and carbon supports will be discussed and compared. Finally, we present a perspective of the promises and challenges of carbon-supported SACs.

2. Sample Preparation

A variety of experimental techniques have been reported in recent literatures for the preparation of carbon-supported



Yi Peng received his B.S. degree in chemistry in 2014 from Beihang University, Beijing, China, and then went on to the University of California at Santa Cruz (UCSC) to pursue a Ph.D. in chemistry under the supervisor of Prof. Shaowei Chen. His research interests include metal/semiconductor nanoparticle surface functionalization, nanoparticle charge-transfer dynamics, and single atom catalysts for electrochemical energy conversion and storage.



Bingzhang Lu received his B.S. degree in chemistry in 2015 from the University of Science and Technology of China (USTC, Class 1103). He is currently a Ph.D. candidate at UCSC under the supervision of Prof. Shaowei Chen and coadvised by Prof. Yuan Ping. His research focuses on the design, synthesis, and DFT calculations of effective electrocatalysts toward new energy conversion devices.



Shaowei Chen received his B.S. degree in chemistry from USTC (Class 8603) in 1991, and his M.S. and Ph.D. degrees from Cornell University in 1993 and 1996, respectively. Following a post-doctoral appointment at the University of North Carolina at Chapel Hill, he started his independent career in Southern Illinois University in 1998. In 2004, he moved to UCSC. He is currently a professor of chemistry and the faculty director of the UCSC COSMOS program. His research interests are primarily focused on high-performance catalysts for electrochemical energy conversion and storage, impacts of metal–ligand interfacial bonding interactions on nanoparticle charge-transfer dynamics, Janus nanoparticles by interfacial engineering, and antimicrobial activity of functional nanomaterials.

SACs, such as pyrolysis, wet chemistry synthesis, physical and chemical vapor deposition, electrochemical deposition, as well as ball milling.

2.1. Pyrolysis

Pyrolysis has been used rather extensively in the preparation of SACs by thermal decomposition of select precursors at elevated temperatures under the protection of a controlled atmosphere (i.e., N_2 , NH_3 , Ar, or H_2). The precursors in general come from five sources, as detailed below.

- (a) *Hybrids of Carbon Matrices and Metal-Containing Complexes*: This is a widely used route to the synthesis of SACs on carbon-based materials. **Figure 1a** schematically illustrates the synthesis of single metal atoms embedded in nitrogen-doped holey graphene frameworks (M-NHGF, M = Ni, Co, and Fe).^[105] Briefly, metal ions-containing porous hydrogels are obtained by hydrothermal treatment of a graphene oxide (GO) solution with metal salts and H_2O_2 . Then the hydrogels are freeze-dried and annealed at elevated temperatures in the atmosphere of NH_3 and Ar, where NH_3 not only serves as the reducing agent but also provides the nitrogen source. In the final products, MN_4 moieties are formed and embedded within the graphene lattice. This method is particularly useful in the synthesis of MN_x (M = Fe, Ni, and Co) moieties in a graphene matrix with nitrogen-free precursors.^[89,91,118] For nitrogen-containing precursors, this method is suitable as well. For instance, RuN_4 moieties have been prepared and incorporated into a graphene matrix by annealing GO nanosheets decorated with $[Ru(NH_3)_6]^{3+}$ due to the strong interactions between the oxygen-containing functional groups of GO and Ru(III) metal cations in an NH_3 flow.^[79] Note that with nitrogen-containing precursors such as hemin, phen, porphyrin, phthalocyanine, melamine, carbon nitride, cyanamide, and 2,3,7,8-tetra(pyridin-2-yl)pyrazino[2,3-g]quinoxaline, NH_3 gas becomes unnecessary and can be replaced by N_2 or Ar.^[84,86,102,119–124] Other SACs have also been synthesized in a similar fashion, such as CoP_4 embedded in C_3N_4 , Co, and P co-doped rGO, PtS_4 in graphitic carbon, as well as single metal atoms (e.g., Ni, Co, NiCo, CoFe, and NiPt) in N-doped carbon nanotubes (CNT) and graphene.^[75,78,125–127]
- (b) *Metal–Organic Frameworks (MOFs)*: In recent years, MOFs have been attracting extensive interest because of the well-defined porous structure and highly ordered arrangement of organic linkers and metal nodes; in addition, MOFs and MOF-derived materials have been widely employed as catalyst precursors or catalysts.^[60,129–133] As the metal species are atomically dispersed in MOFs, SACs supported on carbon can be readily obtained, despite the challenge of metal atom aggregation to form nanoparticles during high-temperature pyrolysis.^[131,134,135] For instance, Li and coworkers showed that during pyrolysis of a Co-containing MOF (e.g., zeolitic imidazolate frameworks, ZIF-67), the organic linkers were converted into N-doped porous carbon and cobalt was reduced by carbon and aggregated, leading to the production of a hybrid consisting of Co nanoparticles incorporated in N-doped carbon (NC).^[96] Yet, when half of the Co in ZIF-67 was replaced by Zn forming the bimetallic counterpart, Zn_1Co_1 -BMOFs, single Co atoms were formed after pyrolysis and embedded in the N-doped carbon matrix. This is because (i) the addition of Zn enlarged the distance between the Co atoms and (ii) the evaporation of Zn at high

temperatures produced an increasing number of nitrogen anchoring sites that stabilized Co (Figure 1b), both of which impeded the formation of Co–Co bonds. Wu's group used a similar method and obtained Co-NC SACs with CoN_4 embedded in a graphitic carbon matrix.^[97] In fact, this method has been adopted as a generic strategy for the synthesis of SACs in a carbon matrix. For instance, Ni and Fe SACs on NC have been prepared by confining Ni^{2+} and Fe^{3+} within the ZIF-8 pores, respectively.^[99–101,108,136] Interestingly, when ZIF-8 is replaced with Co-containing BMOFs, $FeCl_3$ can still be encapsulated in the cavities, producing (Co,Fe)-NC SACs.^[93] Besides ZIF, other MOFs have also been employed for SAC synthesis, such as Ru-NC SACs from Ru-hosted UiO-66 (or UiO-66- NH_2) and Ni-NC SACs from $[Ni_2(L-asp)_2(bipy)] \cdot CH_3OH \cdot H_2O$ (Ni-MOF, asp = aspartic acid, bipy = 4,4'-bipyridine).^[107,137]

- (c) *Polymers*: Recently polymer precursors have also been used to synthesize SACs. For instance, Lou's group prepared Pt-NC SACs in a porous carbon matrix (PCM) (Figure 1c),^[92] where the Pt component was loaded onto the surface of a polydopamine/diblock copolymer (PDA/PS-b-PEO), PDA was then carbonized and PS-b-PEO was removed during the pyrolysis process, resulting in isolated Pt single atoms on a mesoporous carbon matrix. In another study,^[98] Chen and coworkers used phen and polyaniline as dual nitrogen precursors and synthesized Fe-N-C hybrid structures with a graphene-like morphology. The introduction of phen as a precursor not only enhanced nitrogen-doping but also acted as a sacrificial pore-forming agent, because of the relatively low thermal decomposition temperature of phen that facilitated the formation of a significant amount of gas during pyrolysis. The Zelenay group also synthesized SACs with FeN_4 moieties embedded in a graphitic carbon matrix by pyrolysis of dual nitrogen-precursors of polyaniline (PANI) and cyanamide.^[104]
- (d) *Small Molecular Precursors*: This is a straightforward method, but has not been widely used because small molecular precursors usually have relatively low thermal decomposition temperatures, which renders it difficult to carbonize the precursors. To synthesize SACs, the selection of molecular precursors is critical, and thus far most of the precursors are nitrogen-rich. For instance, Chen et al.^[128] used silver tricyanomethanide ($AgTCM$) and cyanamide as the starting molecular precursors and successfully obtained graphitic carbon nitride (C_3N_4) nanosheets doped with individual Ag atoms (Figure 1d). Wang et al.^[138] synthesized C_3N_4 -based SACs co-loaded with Ag single atoms and carbon quantum dots. Gao et al.^[139] pyrolyzed $[Cu_2Cl_2(\mu-Cl)(\mu-OCH_3)(CH_3OH)(MA)_2 \cdot 2Et_2O]$ (MA = melamine) and obtained Cu SACs on C_3N_4 . In another study, Yang et al.^[106] prepared Ni SACs in a nitrogen-doped graphene (NG) matrix and nitrogen and sulfur co-doped graphene (NSG) matrix using melamine, nickel salt, and L-alanine ($C_3H_7NO_2$, for NG) or L-cysteine ($C_3H_7NO_2S$, for NSG) as the precursors.
- (e) *Sacrificial Template-Assisted Route*: Porosity, and hence BET surface area, of SACs can be enhanced during the pyrolysis process by the incorporation of sacrificial templates.^[140–144] For instance, Liang et al. synthesize a family of Co and Fe SACs embedded in mesoporous carbon by using silica

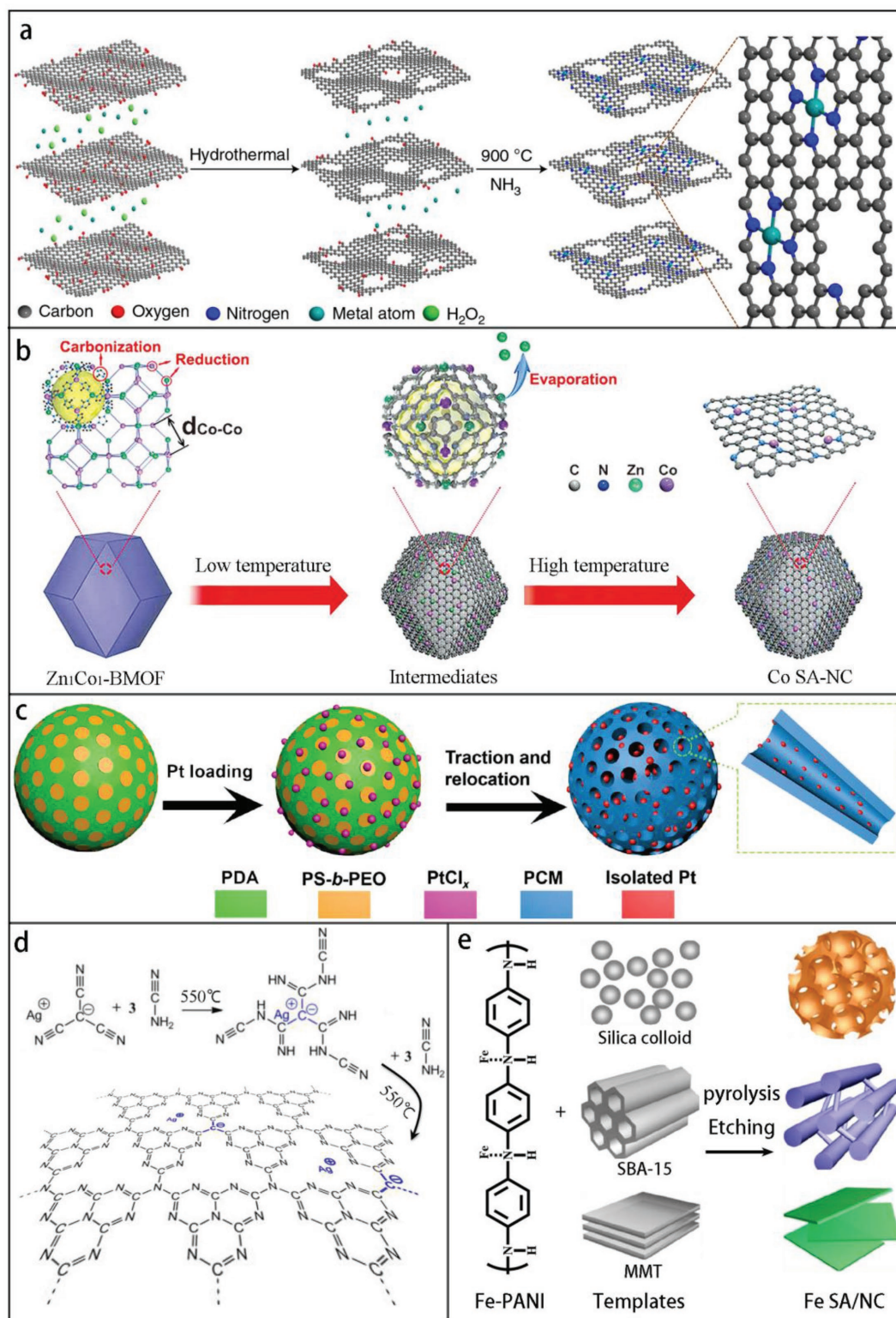


Figure 1. Representative examples of metal SACs supported on a carbon matrix through a pyrolysis route with various precursors. a) Preparation of M-NC (M = Fe, Co, Ni) with MN_4C_4 moieties in which the precursors are metal ions adsorbed on a 3D graphene hydrogel. Reproduced with permission.^[105] Copyright 2018, Macmillan Publishers Limited. b) Preparation of Co-NG from a Zn₁Co₁-BMOF precursor. Reproduced with permission.^[96] Copyright 2016, Wiley-VCH. c) Synthesis of Pt-PCM starting with polydopamine. Reproduced under the terms of the CC-BY 4.0 license.^[92] Copyright 2018, American Association for the Advancement of Science. d) Ag-C₃N₄ derived from silver tricyanomethanide and cyanamide. Reproduced with permission.^[128] Copyright 2016, American Chemical Society. e) Synthesis of Fe-NC with the assistance of various templates. Reproduced with permission.^[95] Copyright 2013, American Chemical Society.

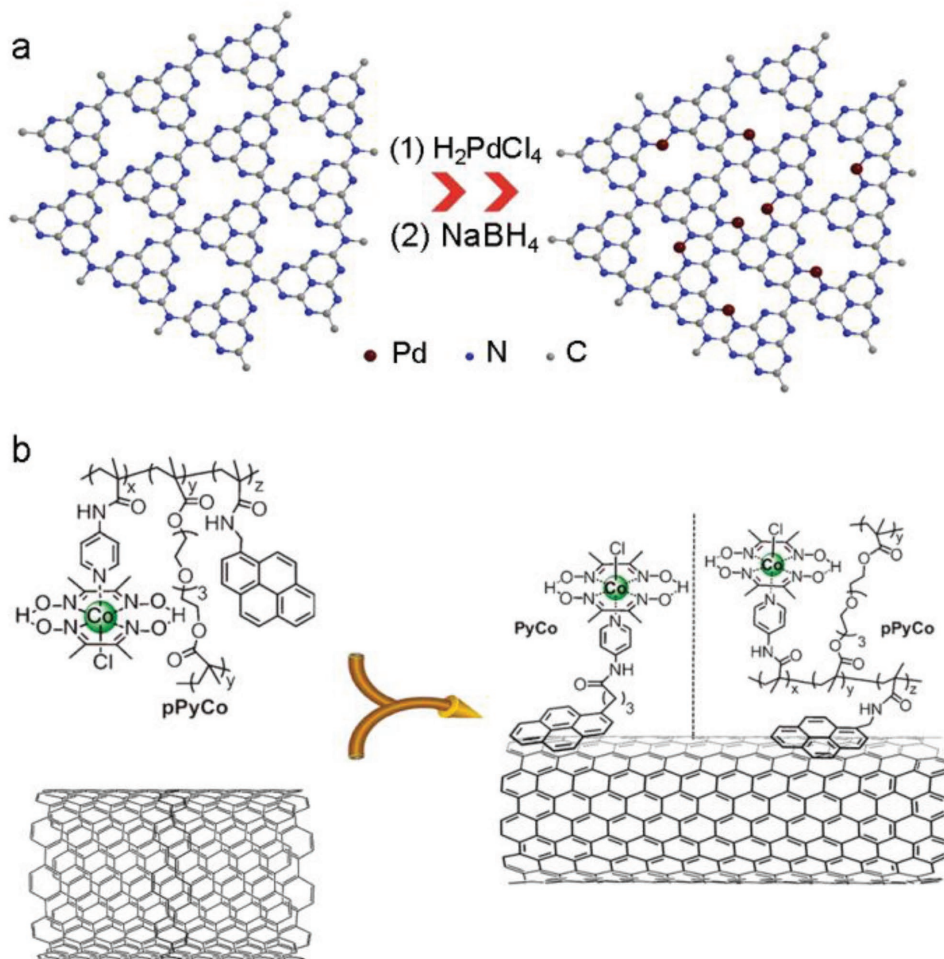


Figure 2. Representative examples of metal SAC supported on carbon-based materials synthesized by wet chemistry routes. a) Pd- C_3N_4 based on a chelation mechanism that Pd atoms are coordinated to N sites. Reproduced with permission.^[147] Copyright 2015, Wiley-VCH. b) Synthesis of Co-CNT based on a host-guest mechanism where the Co complexes are adsorbed on CNT by pyrene moieties. Reproduced with permission.^[74] Copyright, 2016, Wiley-VCH.

colloid, ordered mesoporous silica SBA-15 and montmorillonite clay as sacrificial templates, and vitamin B12 or PANI-Fe as the Co or Fe precursors (Figure 1e). After pyrolysis, the templates were removed by HF etching leading to the generation of CoN_x or FeN_x moieties in a porous matrix.^[93] Silica-based templates have also been used to synthesize FeN_2 moieties in mesoporous carbon and Co SACs in hollow N-doped carbon spheres.^[94,103] Additionally, nano-MgO and $Mg(OH)_2$ have been used as sacrificial templates for the synthesis of FeN_x ($x = 4 - 6$) and CoN_4 moieties in a carbon matrix.^[145,146]

2.2. Wet Chemistry

SACs have also been prepared by wet chemistry routes, primarily involving two slightly different procedures. The first one is based on chelation between metal centers and N, O or S coordination sites in carbon-based materials. For instance, Vile et al.^[147] synthesized Pd SACs supported on mesoporous C_3N_4 by mixing $PdCl_2$ and NaCl in a C_3N_4 dispersion under

magnetic stirring and sonication, followed by $NaBH_4$ reduction (Figure 2a). This was primarily ascribed to the strong coordination between the metal centers and the N sites of C_3N_4 , and the procedure has also been used to prepare Pt- C_3N_4 and Ru- C_3N_4 SACs.^[113,148] In some of the studies, the structure of the metal atoms in the carbon matrix is not clearly defined.^[82,83] For instance, Xi et al.^[149] reported the synthesis of Pd SACs supported on reduced graphene oxide/amorphous carbon (rGO/AC/Pd) by stir-mixing of K_2PdCl_4 with rGO@AC. Whereas Pd was presumed to be intercalated between AC and rGO, the exact chemical structure was unclear.

The other procedure takes advantage of the formation of a guest-host structure through covalent bonds, π - π stacking or electrostatic interactions between the guest molecules and the carbon-based host materials.^[74,76,150-152] For instance, Pt single atoms have been anchored onto thiolated CNTs via covalent Pt-S bonds.^[153] Nickel or cobalt complexes can be grafted onto CNT surfaces by the strong noncovalent π - π stacking interactions between the pyrene moiety in the ligand and CNTs (Figure 2b).^[74,76] Carbon-supported binuclear-cobalt

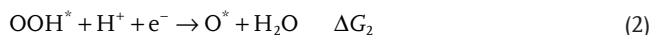
SACs. For instance, using iron phthalocyanine and graphene as the starting materials, Deng et al.^[166] successfully embedded FeN₄ moieties in graphene matrices at high Fe loadings (up to 4.0 wt%). Subsequently, they expanded the study to other metals (i.e., Mn, Fe, Co, Ni, and Cu) by simply using the corresponding metal phthalocyanine as the precursor.^[167]

2.5. Graphene Vacancy-Directed Synthesis

This strategy entails two key steps. The first is to create graphene vacancies by high-energy atom/ion irradiation and control the number of vacancies by the energy density^[168]; and the second is to fill the graphene vacancies with select metal atoms, such as Au, Pt, Fe, Co, and In, by well-controlled sputtering or focused ion beams.^[169–171] The advantage of this strategy includes a well-defined and custom-tailored structure of the final products, allowing a reliable model for theoretical simulations, while the disadvantage entails rather sophisticated instrumentation, tedious fabrication and an extremely low yield (for instance, the preparation is generally limited to a very small area, e.g., 10 nm × 10 nm),^[169] rendering it difficult for scale-up synthesis of practical catalysts.

3. Electrocatalytic Performance

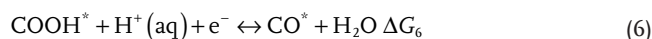
The SACs prepared above exhibit apparent electrocatalytic activity toward various reactions that are critical in electrochemical energy conversion and storage. Theoretical calculations represent a powerful tool in analyzing/predicting the catalytic performance, which can be exploited as a fundamental framework for the rational design and engineering of the catalysts. For instance, in ORR, OER, and CO₂RR, a linear relation (a.k.a. scaling relation) has been widely observed between the binding energy of various critical intermediate species,^[114,172–174] a unique feature that can be used for the manipulation and optimization of the catalytic performance. In ORR, the traditional four-step reaction can be written below (with the corresponding reaction free energies of ΔG₁ to ΔG₄)^[175]



where * represents a catalytic active site. Note that ΔG₂ + ΔG₃ = E_{OH*} - E_{OOH*} + b', where E_{OH*} and E_{OOH*} are the binding energy of the OH and OOH intermediates, respectively, and b' is a constant. In ORR, typically either step (1) or (4) is the rate determine step, and at ΔG₁ = ΔG₄ = ΔG_{ave} (= 1/4ΣΔG_i), the performance of the catalyst is predicted to reach the

maximum. At this point, since ΣΔG_i = -4.92 eV, ΔG₂ + ΔG₃ = -4.92 - (ΔG₁ + ΔG₄), and ΔE_{OH*} - ΔE_{OOH*} = -2.46 - b'. That is, E_{OH*} and E_{OOH*} scale linearly with each other, and from the intercept, b' can be determined, which can then be used to predict the optimal electrode potential (U).

Similarly, in CO₂RR, the first three reaction steps are generally expressed as



When CO is the final product, the rate determine step is either reaction (5) or (7),^[176] and a linear correlation has been observed between E_{COOH*} and E_{CO*}.^[177] With other final products, reaction (8) is the rate-determine step,^[178] and a scaling relation can be found between E_{CHO*} and E_{CO*}.^[177]

Interestingly, such a scaling relation can be broken with SACs,^[173,177] as manifested with a different intercept value. In a previous study,^[114] we showed that in Fe,N-codoped carbon for ORR, the Fe center of FeN₄ exhibited a markedly different linear relation between E_{OH*} and E_{OOH*} from that of regular carbon sites (**Figure 4a**). The smaller intercept corresponded to a more positive onset potential (E_{onset}), in good agreement with experimental results that showed an enhanced ORR performance. Such a deviation from the conventional scaling relation has been observed in other catalytic reactions (e.g., CO₂RR in **Figure 4b**), leading to marked enhancement of the catalytic activity over that without the SAC moiety. Below, we will summarize recent progress in the design and engineering of SACs in ORR, HER, OER, and CO₂RR.

3.1. ORR

Platinum has been the catalyst of choice for ORR. Yet, Pt SACs behave markedly differently than conventional Pt/C catalysts. For instance, Choi et al.^[78] loaded S-doped zeolite-templated carbon with single Pt atoms to form PtS₄ SACs. The sulfur worked as the binding site of Pt that mitigated the aggregation problem of SACs on carbon substrates. Interestingly, the resulting atomically dispersed Pt showed a high yield of H₂O₂, indicating that oxygen underwent only two-electron reduction, in sharp contrast to conventional (bulk) Pt catalysts where four-electron reduction is commonly observed.^[51,179–183] In fact, the sample with the highest PtS₄ concentration showed a H₂O₂ yield of 96% with an E_{onset} of +0.71 V versus RHE in 0.1 M HClO₄. DFT studies indicated that the 2e reduction of oxygen was under kinetic control rather than thermodynamic control, as the reorganization energy (λ₀) for the 2e pathway was markedly smaller than that for the 4e pathway. Consistent

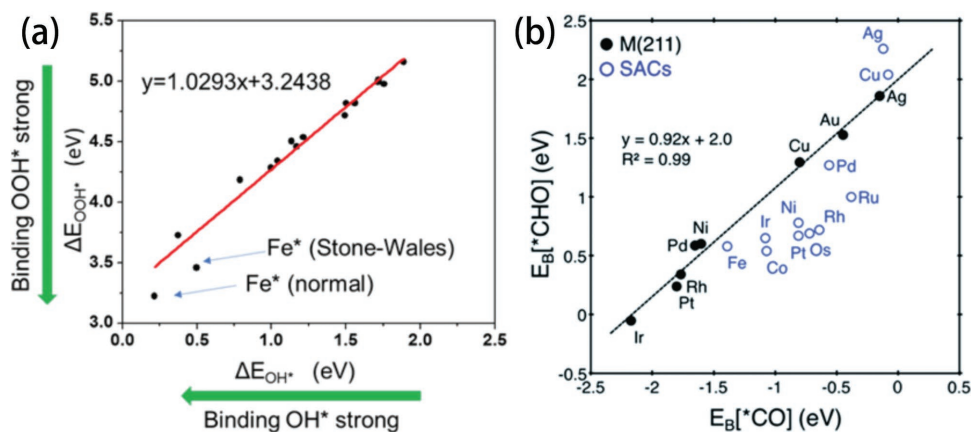


Figure 4. a) $E_{\text{OOH}^*} \sim E_{\text{OH}^*}$ linear relation for ORR. The data points from regular carbon sites follow the linear relation (red line), whereas the two data points beyond the linear range represent single atom Fe centers of FeN_4 . Reproduced with permission.^[114] Copyright 2017, American Chemical Society. b) $E_{\text{CHO}^*} \sim E_{\text{CO}^*}$ linear relation for CO_2RR , where SACs (blue circles) are situated beyond the linear range for metal (211) surfaces (black dots). Reproduced under the terms of the CC-BY 3.0 license.^[173] Copyright 2018, Royal Society of Chemistry.

experimental results were obtained in other studies with Pt SACs supported on TiC, TiN or ATO.^[181] This is because the Pt atoms are the ORR active sites and can adsorb only one O atom of O_2 , which renders it difficult to break the O–O bond; and for four-electron reduction of oxygen to H_2O , the breaking of the O–O bond may be facilitated when two adjacent Pt sites are available to adsorb both two O atoms of O_2 . In addition, DFT calculations suggest that the interaction between Pt single atoms and TiN increases the affinity of oxygen species onto the catalysts and thus diminishes the catalytic activity.

SACs of other noble metals have also been examined as ORR catalysts. Zhang et al.^[79] developed a Ru SAC for ORR by thermally annealing Ru compounds and N-doped carbon. EXAFS and high-resolution scanning TEM studies suggested successful formation of RuN_4 moieties in the structure, which exhibited a high ORR activity in acid electrolytes. The E_{onset} and $E_{1/2}$ (half-wave potential) values were identified at +0.89 V and +0.75 V versus RHE, respectively, a performance better than that of FeN_4 and very close to that of commercial Pt/C. DFT study showed that the binding of the Ru center in RuN_4 with O was responsible for the ORR activity, and the rate-determine step was likely the protonation of O_2 that was adsorbed onto the Ru site.

Non-noble metal SACs have also been examined as ORR catalysts. For instance, Lee et al.^[184] synthesized Fe-doped CNTs with a FeN_4 structure by a conventional plasma-enhanced CVD method, and the material possessed apparent electrocatalytic activity toward ORR. XPS studies showed a Fe:N:C atomic ratio close to 1:4:100, which was consistent with results from the formation energy calculations, where the content of the Fe dopant was found to diminish with decreasing N concentration in CNTs. Results of band structure calculations suggested that FeN_4 and other nitrogen dopant defects enhanced the electrical conductivity over pristine CNTs, due to the shift of the Fermi level, the formation of new states ≈ 0.3 eV above the Fermi level by the FeN_4 moieties, and spin-polarization effect. The shift of the Fermi level was favorable for the adsorption of intermediate

species, although there was no explicit discussion in the studies about the correlation with the activity of the catalyst.^[175,185] Recently, similar structures were further examined theoretically with the advancements of the ORR mechanism. For instance, Wang et al.^[186] used iron-phthalocyanine (Fe-Pc) as an analogue to FeN_4 and calculated the ORR activity with a 2×2 supercell for a Fe-Pc monolayer in an acidic environment. It was found that O_2 could readily bind to the Fe center with charge transfer from Fe to O_2 , and O_2^* reduction was identified to be the rate-determine step. The results showed that the four-electron pathway was favored on Fe-Pc , with an activity between those of N-doped carbon and Pt. In another study,^[187] the metal- N_4 structure was systematically evaluated by including metals of groups 6B, 7B, 8, 1B and 2B. The results showed that MN_4 of the Mn, Fe, and Co group metals exhibited apparent activity toward ORR, with the adsorption of OOH and release of OH being the rate determine steps. We observed similar behaviors in an early study.^[114] We calculated the free energy change of every elementary step in ORR in a wide range of structural configurations of N-doped graphene and FeN_4 -embedded graphene. The most active configurations are shown in Figure 5a,b, where the Fe center of FeN_4 exhibited a much higher activity (with a reaction free energy as low as 0.39 eV) than carbon atoms of N-doped graphene (reaction free energy at least 0.61 eV). Moreover, from the DOS plots (Figure 5c,d), it can be seen that the number of states around the Fermi level was significantly higher for the FeN_4 moiety than for neighboring nitrogen and carbon, with dominant contributions from the Fe 3d orbital. This indicates that the Fe center is favorable for the adsorption of O_2 and may donate electrons to reduce O_2 , in contrast to the adjacent carbon sites.

Such mechanistic insights suggest that in metal and nitrogen-codoped carbon, the MN_4 moieties play a dominant role in ORR electrocatalysis and are most likely the ORR active sites.^[95] It should be noticed that this topic has been under active debates and intensive investigations.^[188–191] For instance, Chen et al.^[99] used ZIF-8 to trap $\text{Fe}(\text{acac})_3$, and pyrolysis of the resulting structure yielded single Fe atoms embedded

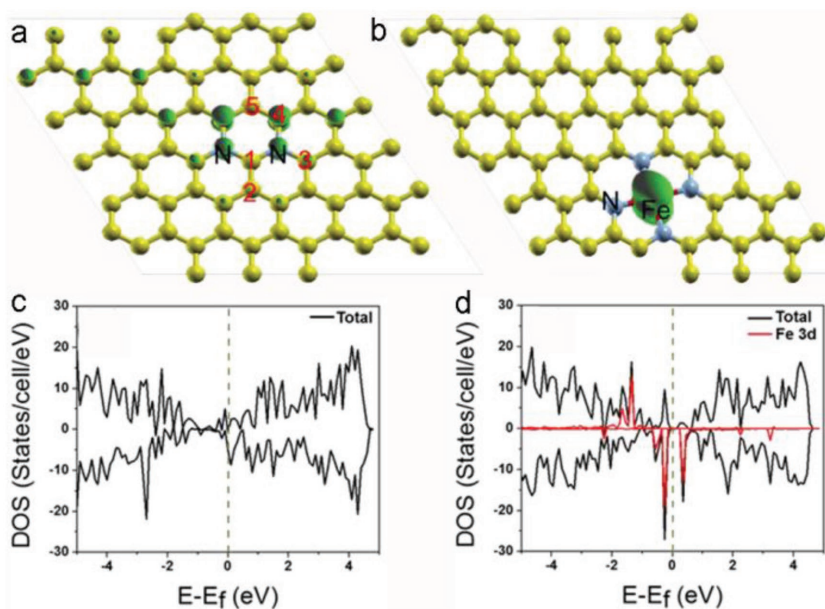


Figure 5. a,b) Calculation models of nitrogen-doped graphene (a) and FeN₄-embedded graphene (b). c,d) DOS plots of N-doped graphene (c) and FeN₄ embedded graphene (d). Reproduced with permission.^[114] Copyright 2017, American Chemical Society.

within the carbon skeletons. From **Figure 6a,b**, single Fe atoms (marked with red circles) can be seen to be distributed rather evenly across the carbon matrix, and the structure is further confirmed by EXAFS measurements (**Figure 6c**). The peak at ≈ 1.5 Å is consistent with the Fe–N bond, and the absence of any peak at ≈ 2.2 Å indicates no Fe–Fe bond in the sample. Moreover, from EXAFS fitting, the coordination number of Fe was estimated to be 5 with a mean bond length of 2.01 Å, consistent with the FeN₄ structure with the adsorption of an O₂ molecule (**Figure 6d**). The resulting sample showed an ORR activity even better than that of Pt/C, with E_{onset} and $E_{1/2}$ estimated to be +0.99 V and +0.90 V, respectively (**Figure 6e**). In poisoning tests with SCN[−], these potentials were found to shift cathodically by 90 mV and 95 mV, respectively (**Figure 6f**), which further proved that the Fe center was the active site for ORR. In another study,^[104] Chung et al. used atomic-resolution STEM to identify single Fe atoms in carbon, and qualitatively estimated the Fe:N ratio by EELS measurements, which suggested an average composition of FeN₄. They argued that the FeN₄ sites near the edge of the graphene layers were the major contributors to the ORR activity.

Consistent results have also been observed in other studies.^[87,98,100,101] However, it has been noted that in Fe-NC materials, the presence of Fe and peroxide (an ORR intermediate) may cause degradation of organic ionomers and fuel cell membranes due to Fenton reaction.^[192,193] To mitigate this issue, Co-NC materials have been designed and fabricated. For instance, Wang et al.^[97] used ZIF doped with different concentrations of Co to fabricate Co-NC SACs, and attributed the ORR activity to the CoN₄ moieties.

In some other studies, the ORR activity of MNC hybrids is actually ascribed to the metal center of an MN₂ moiety. For instance, Shen et al.^[103] used SBA-15 as a template, FeCl₃,

ethylenediamine, and carbon tetrachloride as the Fe, N, and C source, and synthesized Fe SACs for ORR by pyrolysis, which were denoted as FeN₂/NOMC. HAADF-STEM (**Figure 7a,b**) and elemental mapping (**Figure 7c,d**) studies showed that Fe atoms were dispersed individually within the carbon structure. EXAFS and Mossbauer spectroscopic measurements suggested the formation of FeN₂ moieties. Specifically, results from EXAFS measurements (**Figure 7e**) confirmed the formation of Fe–N bonds, but no Fe–Fe in the sample, and the Fe coordination number was estimated to be 2. Since no coordination of oxygen or carbon to iron was observed in Mossbauer measurements (**Figure 7f**), it was argued that the Fe center was in the form of FeN₂. Interestingly, the resulting material exhibited a remarkable ORR activity in alkaline solutions with $E_{1/2} = +0.863$ V (**Figure 7g**), suggesting a lower overpotential than that of FeN₄. In another study,^[96] CoN_x SACs were prepared by pyrolysis of Zn/Co BMOFs with $E_{1/2} = +0.881$ V. EXAFS studies showed that CoN₄ dominated the ORR activity for the sample prepared at

800 °C, and the ORR activity was even better for the sample prepared at 900 °C which consisted mainly of CoN₂.

Durability is another important factor in the evaluation and comparison of catalytic performance. For instance, Wang et al.^[97] carefully examined the durability of CoN₄ SAC embedded in a 3D porous MOF-derived carbon matrix (Co-N-C) as ORR catalysts in PEMFC. The long-term stability test was carried out by potential cycling in the potential range of +0.6 to +1.0 V at the potential scan rate of 50 mV s^{−1}, and the results showed that $E_{1/2}$ shifted only by 30 mV after 10 000 cycles (**Figure 8a**). In addition, in chronoamperometric tests, 83% of the initial activity was retained after continuous operation for 100 h at +0.7 V (**Figure 8b**). Note that for commercial Pt/C, the current density decreased to about 80% after only ≈ 20 h.^[194] The durability of the catalyst was also tested in PEMFC using a cathode fed by air for 100 h at the fully viable voltage of 0.7 V (**Figure 8c**). **Figure 8d** depicted the voltage-current polarization plots. One can see that the voltage loss was only 15 mV after 30 h and 60 mV after 100 h. These tests demonstrated excellent long-term stability of the Co-N-C catalyst. For SACs, one issue is that the metal single atoms are not stable in the structure, and aggregation and/or dissolution may diminish the activity and durability. For the Co-N-C catalyst, aberration-corrected HAADF-STEM studies of the sample after 10 000 potential cycles (**Figure 8e,f**), along with EEL point spectral analysis (**Figure 8g**), showed that the 3D carbon architecture was well-retained, Co single atoms remained well-defined, and both Co and N could be readily detected, indicating sufficient stability of the Co-N-C catalyst in acidic media. Remarkable stability has also been observed in several other studies in either alkaline or acidic electrolyte,^[93,94,98,99] although no detailed characterization of the catalysts was included after the durability test, and the structural integrity of the catalysts remained unknown.

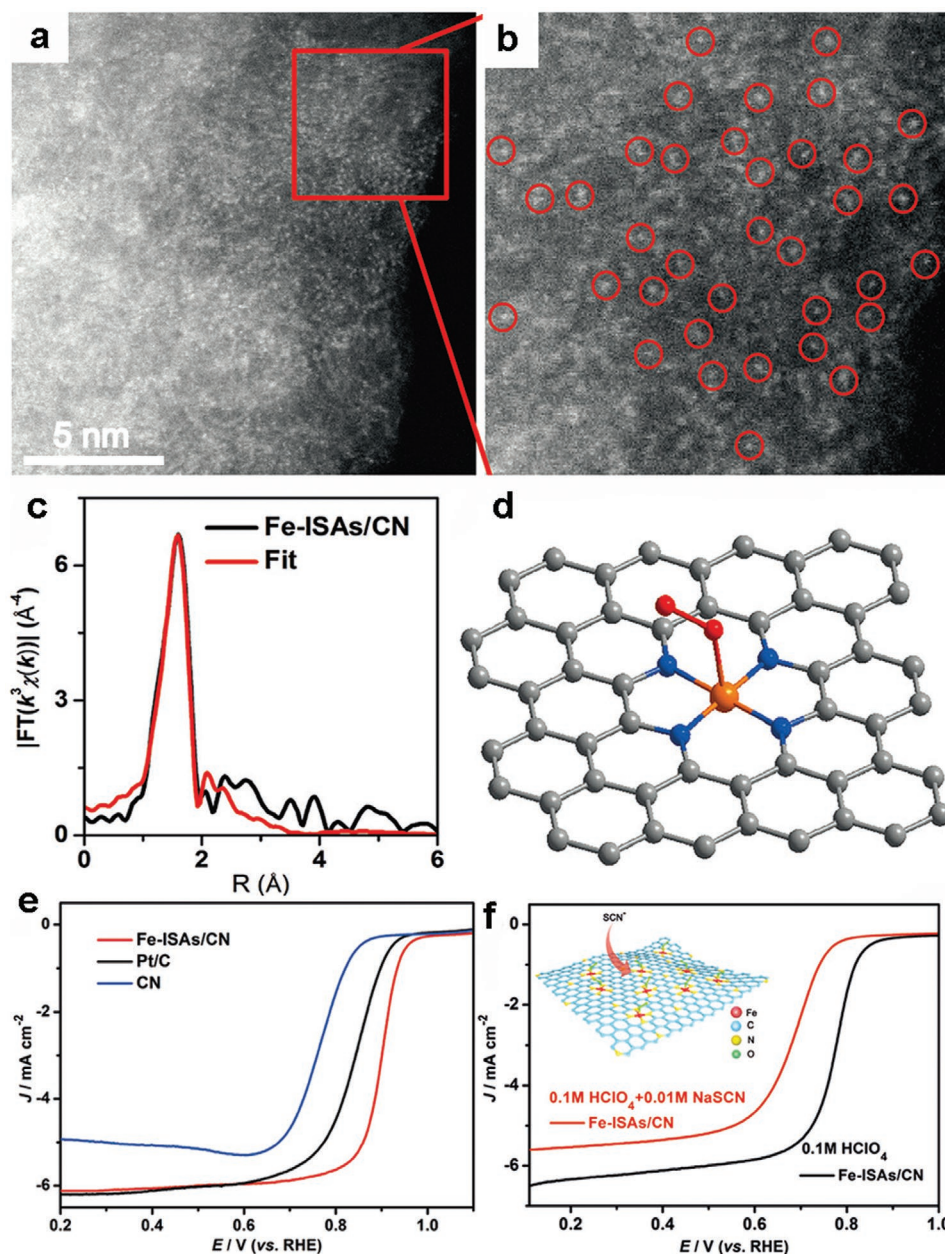


Figure 6. a) TEM image of Fe-trapped ZIF-8 after high-temperature treatment. b) HRTEM image of single atom Fe (highlighted by red circle), c) EXAFS *r* space fitting curves of single Fe atoms of Fe-ISAs/CN, and d) its schematic model, Fe (orange), O (red) and C (grey). e) LSV curve of Fe-ISAs/CN, Pt/C and sample without single atom Fe (named as CN). The data were taken in 0.1 M KOH. f) LSV curve of Fe-ISAs/CN acquired in 0.1 M HClO₄ with and without 0.01 M NaSCN. Reproduced with permission.^[99] Copyright 2017, Wiley-VCH.

In summary, thus far studies have been mainly focused on two kinds of SACs for ORR. One is single atoms of noble metals such as Pt and Pd, and the other is MN_x moiety embedded in a carbon matrix. For Pt SACs, ORR is dominated by the two-electron pathway and generates H₂O₂ as the final product, instead of H₂O or OH⁻. Meanwhile, the onset potential exhibits an apparent cathodic shift, as compared to that of commercial Pt/C, suggesting impeded electron-transfer kinetics in oxygen reduction, likely due to restricted adsorption of oxygen onto the single Pt atomic site. For SACs with the MN_x structures, the metal centers are generally believed to be responsible for the ORR activity, although

the coordination number may vary due to different synthetic procedures. Consistent results are obtained in DFT studies within the context of adsorption energy of oxygen species on various atomic sites and contributions to the DOS near the Fermi level.

3.2. HER

The first heterogeneous catalysts for HER are based on “host-guest” structures where single metal centers are hosted on the surface of conductive carbon materials by covalent^[151,152] or

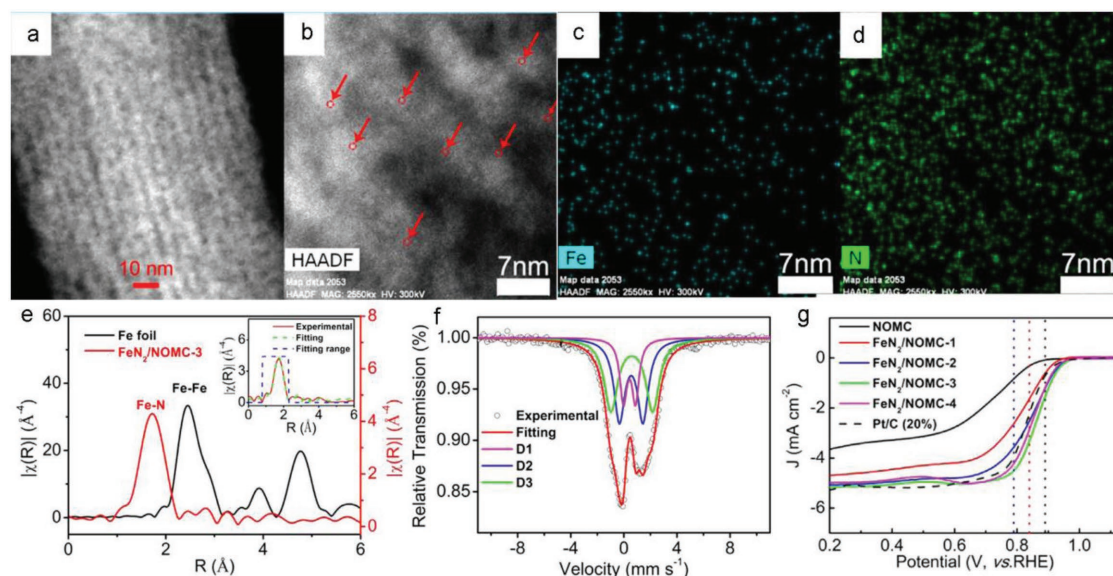


Figure 7. a,b) HAADF-STEM of FeN₂/NOMC-3 on carbon, and c,d) EELS mapping analysis of Fe (c) and N (d). e) Fourier-transformed EXAFS spectra of FeN₂/NOMC-3. f) Fe⁵⁷ Mössbauer spectra of Fe⁵⁷N₂/NOMC-3. g) ORR polarization curves of NOMC, FeN₂/NOMC (20%) at 1600 rpm in an O₂-saturated 0.1 M KOH solution at the potential scan rate of 10 mV s⁻¹. Reproduced with permission.^[103] Copyright 2017, Elsevier Ltd.

noncovalent bonds.^[74,76,150] In a recent study, inspired by hydrogenases,^[195–198] nickel bisdiphosphine was assembled onto CNT surfaces,^[199] which exhibited high catalytic activity toward HER, with an onset potential of only -20 mV and almost unchanged current density after continuous operation for 10 h. In another study,^[74] a hybrid of ploy(cobaloxime) and CNTs was prepared by π - π interactions between CNTs and the pyrene moiety which was tethered to ploy(cobaloxime). The hybrid catalyst possessed an apparent activity toward HER at near-neutral pH, with the cobalt-based turnover number up to 420, about four times higher than that of monomeric cobaloxime. Obviously, in this type of HER catalysts, the metal centers work as the active sites for HER, while the carbon materials are used as the conducting support. As the structures are well defined, relevant structural models can be readily built for computational studies for a coherent understanding of the reaction mechanism. However, the catalytic performance is generally subpar as compared to those of benchmark catalysts like Pt/C.

More recently, carbon-supported SACs based on single atoms of non-noble metals (e.g., Fe, Co, Ni, and Cu) have been prepared and examined for HER electrocatalysis. For instance, the Tour group synthesized single Co atoms incorporated in nitrogen-doped graphene (Co-NG) or undoped graphene (Co-G) via a pyrolysis process.^[91] In dark-field TEM measurements (Figure 9a), the white spots of 2 to 3 Å in size are the dispersed Co atoms, whereas Fourier-transformed EXAFS studies (Figure 9b) showed only a major peak at ≈ 1.5 Å for both Co-NG and Co-G, and waveket-transformed EXAFS studies (Figure 9c) showed a maximum (point A) at 3.2 Å⁻¹ and 3.5 Å⁻¹, due to the formation of Co–C and Co–N bonds in Co-G and Co-NG, respectively, confirming the formation of single Co atom structure in the samples.^[200] In HER tests, Co-NG showed an excellent performance, with an onset potential of only -30 mV, and an overpotential (η_{10}) of -140 mV to reach the current density of 10 mA cm⁻², in comparison to

NG and Co-G where $\eta_{10} \approx -440$ mV and -390 mV, respectively (Figure 9d). In fact, the HER performance of Co-NG was higher than or comparable to results of relevant catalysts in the literature (Figure 9e).^[166,201–206] In another study,^[107] Ni-NC SAC was also found to possess excellent HER performance.

Interestingly, when single Ni atoms were embedded into a (undoped) graphene matrix, apparent HER activity was also observed.^[90] DFT calculations evaluated the energetic properties of several possible configurations, such as interstitial Ni in the center of the phenyl rings (Ni_{ab}), substitutional doping at the vacancy of the graphene lattice (Ni_{sub}), and anchoring on the defect sites (Ni_{def}). The results (Figure 10a,b) showed that all these configurations exhibited a decrease of the absolute Gibbs free energy of hydrogen adsorption ($|\Delta G_{H^*}|$) at carbons neighboring the Ni atoms, as compared to that of pristine graphene. Notably, the $|\Delta G_{H^*}|$ of carbons adjacent to Ni_{sub} was only 0.10 eV, very close to that of Pt (0.09 eV). This was contributed to charge transfer between Ni_{sub} (d orbitals) and surrounding carbons (sp orbitals), resulting in the formation of an empty C-Ni hybrid orbital close to the Fermi level and hence the formation of a catalytic active site (Figure 10c,d). In the studies by Muralikrishna et al.,^[207–209] single Cu atoms were chelated to GO, and the corresponding HER performance was better than those of other copper-based HER catalysts.

Single Pt atoms supported on carbon-based materials have also been prepared and evaluated for HER electrocatalysis. Cheng et al. compared Pt SACs and Pt nanoclusters loaded on nitrogen-doped graphene nanosheets (Pt₁-NG and PtNC-NG, respectively).^[77] Interestingly, both Pt₁-NG and PtNC-NG exhibited higher activities than commercial Pt/C. The DOS plot of Pt₁-NG shows a strong overlap of the Pt 5d orbital and N 2p orbital around the Fermi level. Bader charge analysis shows that Pt was positively charged, and when two hydrogen atoms were adsorbed on the Pt, there is a strong overlap of the Pt 5d and

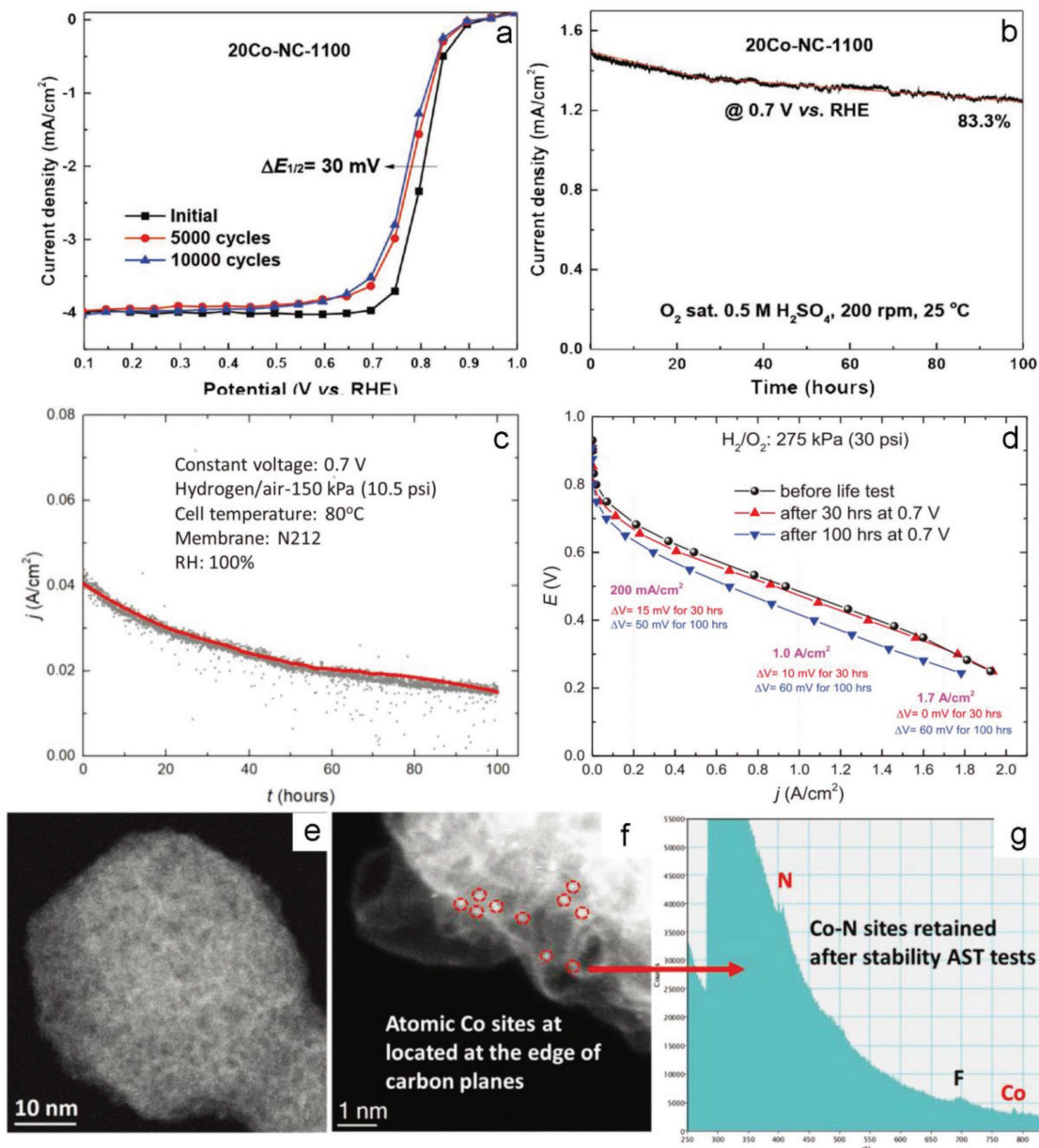


Figure 8. Durability tests of Co-NC SACs as oxygen reduction catalysts in PEMFC. a) Potential cycling in O_2 -saturated 0.5 M H_2SO_4 in the potential range of +0.6 to +1.0 V. b) Chronoamperometric profile at the potential at +0.7 V. c) PEMFC test under H_2 -air conditions at +0.7 V, 150 kPa for 100 h. d) H_2 - O_2 polarization curves before and after 30 h and 100 h durability tests at +0.7 V. e-g) Representative aberration-corrected HAADF-STEM images at low resolution (e) and high resolution (f), and the corresponding EEL point spectra (g). Reproduced with permission.^[97] Copyright 2018, Wiley-VCH.

H 1s orbitals, along with the formation of a number of new states beyond the Fermi level, indicating charge transfer from Pt to H, a critical process in proton reduction. The Lou group further studied the HER performance on Pt SACs in a PCM, where EXAFS and DFT studies indicated that both Pt atom centers and the adjacent carbon/nitrogen atoms were likely the active sites, due to charge density redistribution.^[92] Chen et al.^[210] synthesized Mo SAC catalysts anchored on N-doped carbon by a pyrolysis process using Na_2MoO_4 and chitosan as precursors, and the materials exhibited an η_{10} of only -132 mV, much lower than β - Mo_2C (-195 mV) or MoN (-225 mV). EXAFS studies showed that Mo was threefold

coordinated by one N atom and two C atoms ($MoNC_2$), similar to the above mentioned structure of Ni_{sub} ^[90] but with O_2 adsorbed onto Mo. DFT calculations showed that $MoNC_2$ possessed the lowest $|\Delta G_{H^*}|$, as compared to N-doped graphene, MoN, and β - Mo_2C , consistent with experimental results. Results from DOS calculations indicated a higher electronic density of $MoNC_2$ near the Fermi level, a feature beneficial for HER charge transfer. PDOS studies showed that the charge density was mainly due to Mo d-orbital, while contributions from the p-orbitals of C and N were negligible. This suggests that the enhanced catalytic performance of $MoNC_2$ was largely ascribed to Mo single atoms, with minimal

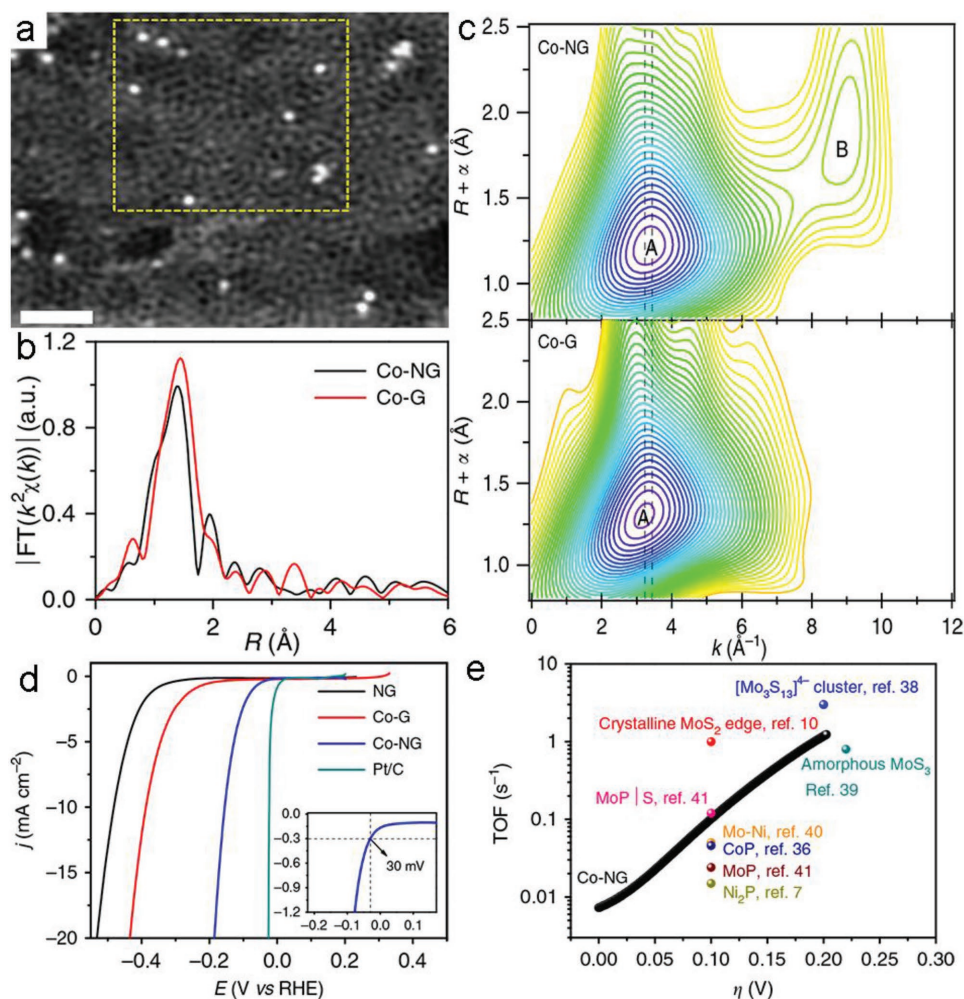


Figure 9. a) HAADF-STEM image of the Co-NG, exhibiting well-dispersed Co atoms in the carbon matrix; scale bar 1 nm. b) Fourier-transformed k^2 -weighted EXAFS spectra in R space for the Co-NG and Co-G samples. c) Wavelet-transformed k^2 -weighted EXAFS spectra for the Co-NG and Co-G samples. d) LSVs of Co-NG and other catalysts in 0.5 M H_2SO_4 at the potential scan rate of 2 mV s^{-1} . The inset depicts the zoom-in LSVs for Co-NG near the onset region. e) Comparison of TOF values of the Co-NG catalyst (black line) with others in recent literature (references cited are those in the original article). Reproduced under the terms of the CC-BY 4.0 license.^[91] Copyright 2015, Macmillan Publishers Limited.

contributions from the C and N coordination sites. Note that this is different from other $\text{MN}_x\text{C}_{4-x}$ or Ni_{sub} structures where the enhanced catalytic performance is mostly accounted for by the interaction between the metal centers and N, C coordination atoms.

In a recent study,^[113] the Chen group showed that Ru ions-complexed C_3N_4 exhibited a remarkable HER performance, due to the formation of RuN_2 moieties, where the interaction between the pyridinic nitrogen of C_3N_4 and Ru metal center led to charge redistribution of the system and facilitated the adsorption of protons. In a subsequent study,^[111] it was found that the performance might be markedly improved by incorporating rGO nanosheets into the Ru- C_3N_4 catalyst by a wet-chemistry route (Figure 11a), with η_{10} of only about -80 mV (Figure 11b). Double-layer capacitance measurements (Figure 11c,d) showed that the effective electrochemical surface area of Ru- $\text{C}_3\text{N}_4/\text{rGO}$ was dramatically enhanced, most likely due to enhanced electrical conductivity of the composite with the incorporation of rGO,

as manifested by electrochemical impedance measurements (Figure 11e), where the serial resistance (R_s) was estimated to be 7.9, 10.0, and 35.4 Ω for Ru- $\text{C}_3\text{N}_4/\text{rGO}$, $\text{C}_3\text{N}_4/\text{rGO}$, and C_3N_4 , respectively. Mott-Schottky analysis (Figure 11f) showed that the flat-band potential (E_{fb}) was virtually unchanged for Ru- $\text{C}_3\text{N}_4/\text{rGO}$ and $\text{C}_3\text{N}_4/\text{rGO}$, but shifted anodically as compared to that of C_3N_4 , indicating narrowing of the energy barrier of hydrogen evolution (H^+/H_2 , 0.59 V vs Ag/AgCl in 0.1 M Na_2SO_4).^[211] Furthermore, the charge-carrier density of Ru- $\text{C}_3\text{N}_4/\text{rGO}$ was about 250 times of that of C_3N_4 and 6 times of that $\text{C}_3\text{N}_4/\text{rGO}$. These results highlight the synergetic effects between the various structural components on the HER performance.

In short, a large variety of SACs for HER have emerged in recent studies. Results have shown that the single metal atoms serve as the active sites, and the activity may be further enhanced by the carbon supports due to interfacial charge transfer with the metal centers, leading to the generation of additional catalytic active centers.

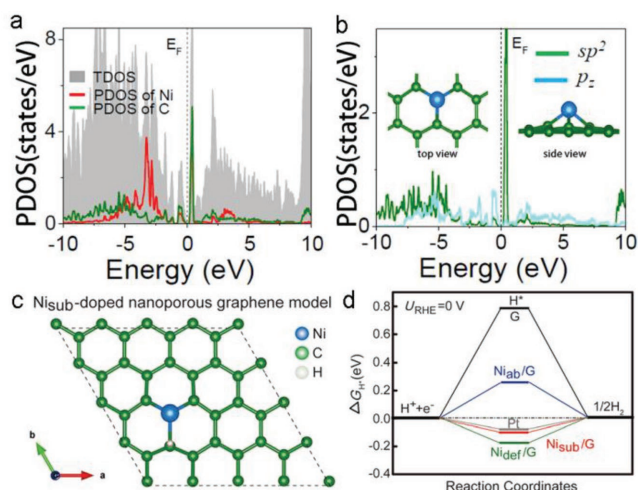


Figure 10. a) DFT calculations of TDOS and PDOS projected to the Ni_{sub} atom (red lines) and the adjacent C atoms (green lines) with optimized structures. b) Orbital-dependent PDOS of the adjacent C atoms in the Ni-G. Inset is the side view and top view of the Ni_{sub} atom in the graphene lattice. c) Hydrogen adsorption sites and configuration of the Ni_{sub}-G model. d) Calculated ΔG_{H*} of HER at equilibrium of various catalysts. Reproduced with permission.^[90] Copyright 2015, Wiley-VCH.

3.3. OER

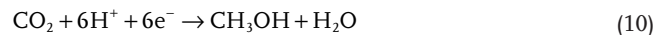
The application of SACs supported on carbon-based materials in OER electrocatalysis has been rarely reported. In an early study,^[83] Jahan et al. described the OER activity of Cu SAC coordinated into a GO-MOF structure. Wurster et al.^[121] found that the OER activity was nonlinearly dependent on the coordination positions of Fe and Co in a supramolecular structure. Ding et al.^[73] developed a sandwich structure where CNT was coated with a uniform layer of polymerized ionic liquids (PIL), and Co atoms were dispersed at the interface. The resulting Co-PIL-CNT SACs showed much better OER catalytic activity than Co₃O₄/CNT and CoCO₃ despite a much lower Co content. This enhancement was ascribed to the combined contributions of the three different components, where Co atoms acted as the active sites, PIL not only served as the anchors for Co SACs but also affected the charge density distribution of Co species leading to enhanced catalytic activity, and CNT provided good electrical conductivity.

More recently, Fei et al.^[105] investigated the MN₄C₄ (M = Fe, Co, and Ni) moieties in a graphene matrix by DFT calculations and experimental studies. Both the M and C in MN₄C₄ moieties were considered as possible active sites and a four-step reaction mechanism were analyzed based on prior studies.^[213,214] Interestingly, the OER process was found to be highly dependent on the metal center in MN₄C₄. For M = Fe or Co, the reaction mechanism was via the single site of the metal center because the binding between M and the intermediates was much stronger than the adjacent C sites (Figure 12a). By contrast, for M = Ni, the reaction mechanism involved both Ni and C sites, and the C sites were favorable for O* and OH* adsorption while the Ni site was preferred for OOH* adsorption (Figure 12b). Figure 12c depicts the calculated energy diagram of OER at 1.23 V for the various MN₄C₄ moieties, and

the results suggested a diminishing activity trend of Ni > Co > Fe, with a totally different rate-determining step, which was oxidation of O* to OOH*, oxidation of OH* to O*, and the formation of OOH*, respectively. A consistent changing trend was indeed observed in electrochemical measurements, where η₁₀ was estimated to be 331 mV for NiN₄C₄, 402 mV for CoN₄C₄, and 488 mV for FeN₄C₄ (Figure 12d); and the Tafel slopes varied accordingly at 63, 80, and 164 mV dec⁻¹ (Figure 12e), respectively. Note that the OER performance of NiN₄C₄ was actually comparable to those of Ni-based nanoparticle catalysts.^[215–218]

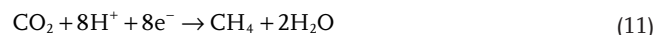
3.4. CO₂RR

Gao et al.^[109] constructed a structural model with single Pd and Pt atoms embedded in C₃N₄ cavities and calculated their electrocatalytic behaviors in CO₂ reduction. They showed that the ideal geometry for the deposition of metal atoms is the center of a sixfold cavity, i.e., position 1 in Figure 13a. Moreover, both Pd and Pt show strong electronic interactions with neighboring pyridinic nitrogen. Specifically, charge is depleted from the Pd d-orbital of Pd-C₃N₄, while both charge accumulation and depletion happen on Pt in Pt-C₃N₄ (Figure 13b,c). CO₂ could be electroreduced to HCOOH, CH₃OH and CH₄. Figure 13b shows the energy diagram of CO₂ reduction catalyzed by a Pd-C₃N₄ SAC, where reduction of CO₂ to HCOOH and CH₃OH was both investigated. The reactions are summarized as follows



While reaction (10) follows the first two steps of reaction (9), the rate-determine step of reaction (9) is hydrogenation of HCOOH* adsorbed onto the Pd atom, with an energy barrier of 0.66 eV. By contrast, the rate-determine step of reaction (10) is hydrogenation of CH₂OH species adsorbed onto the Pd atom, with a much larger energy barrier of 1.46 eV. This result indicated that the Pd-C₃N₄ is favorable to produce HCOOH instead of CH₃OH.

Figure 13c shows the energy diagram of CO₂ reduction catalyzed Pt-C₃N₄. In addition to reactions (9) and (10), the pathway to CH₄ is also under consideration:



Note that reaction (11) follows the first 6 steps of reaction (10). Pt-C₃N₄ shows a significantly different behavior in catalyzing reaction (9) than Pd-C₃N₄. The energy barrier of hydrogenation of HCOOH* is 1.01 eV of the former, much higher than that of the latter; a similar behavior was observed with the HCOOH* desorption energy (1.06 eV for Pt-C₃N₄ and 0.46 eV for Pd-C₃N₄). This indicates that Pt-C₃N₄ is unfavorable to produce HCOOH from CO₂ reduction. However, once HCOOH* is formed, the hydrogenation of other species is much easier than Pd-C₃N₄. Thus, Pt-C₃N₄ can catalyze both reactions (10) and (11). Among these two reactions, CH₂*+H₂O* is more stable than CH₃OH* by 0.47 eV, suggesting that the CH₄ path

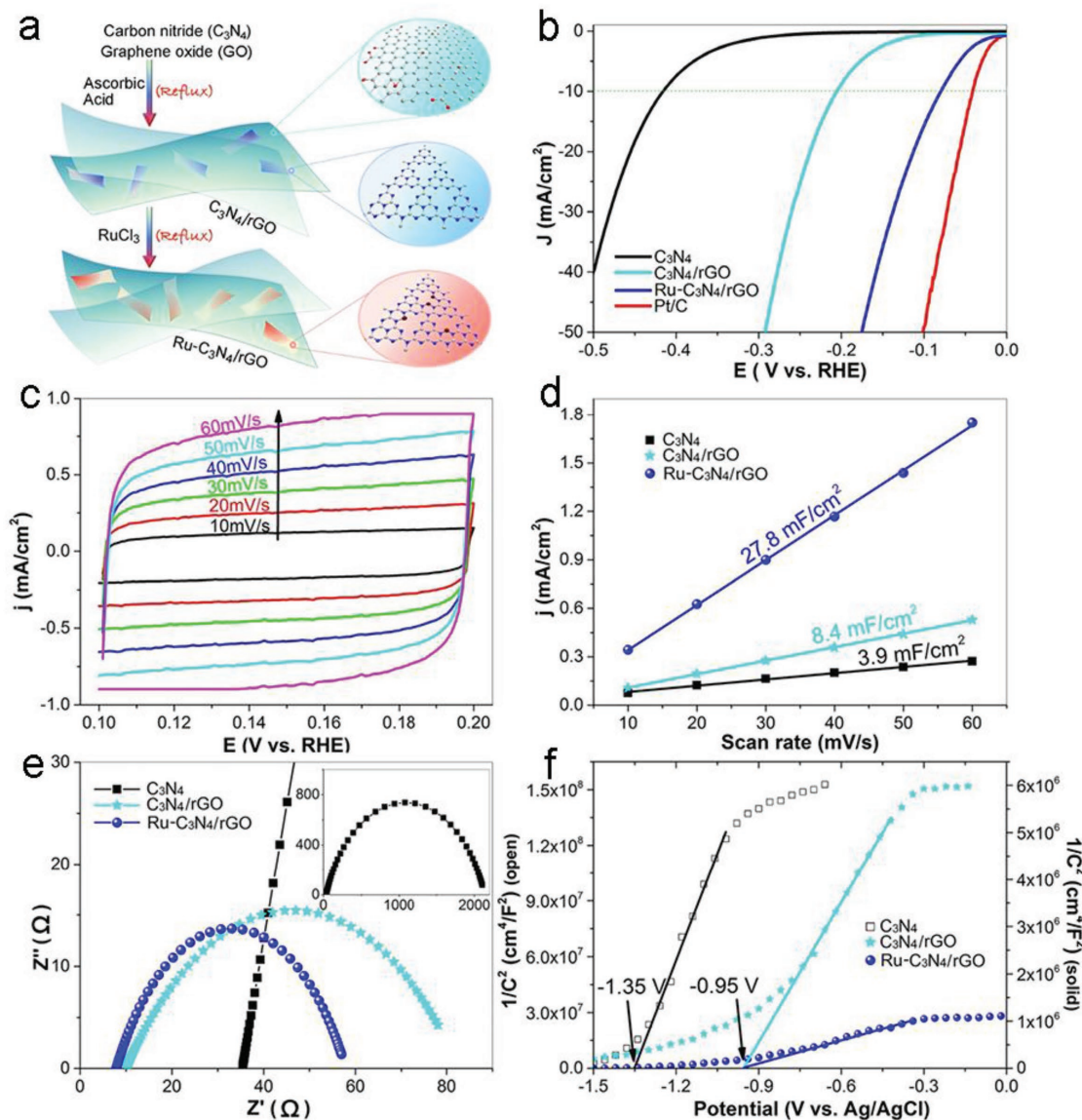


Figure 11. a) Schematic illustration of the synthesis of RuSA-C₃N₄/rGO nanocomposites. b) LSV curves of various electrocatalysts in 0.5 M H₂SO₄. c) CV curves recorded at various scan rates in the potential range without faradaic reaction. d) Capacitive currents as a function of scan rates at +0.15 V. e) Nyquist plots of the various electrocatalysts in 0.5 M H₂SO₄ at -0.1 V. Inset is the full plot of C₃N₄. f) Mott-Schottky plots of the various electrocatalysts in 0.1 M Na₂SO₄ at the frequency of 1000 Hz. Reproduced with permission.^[111] Copyright 2018, Wiley-VCH.

is more favorable. In summary, electroreduction of CO₂ to HCOOH is favorable when catalyzed by Pd-C₃N₄, whereas the path to CH₄ is favored when catalyzed by Pt-C₃N₄.

Relevant DFT calculations have also been carried out recently. He et al.^[113] calculated the energetic characteristics of single metal atoms (e.g., Ag, Cu, Pd, Pt, and Co) supported on defective carbon in CO₂RR to C₁ products. They found that Ag might serve as a promising catalyst in reducing CO₂ to CH₄ while Pt shows a good activity in CO₂RR to CH₃OH. Using a very similar SAC model, Back et al.^[173] showed that carbon-supported SACs exhibited enhanced selectivity for CO₂RR, as compared to HER. In particular, Ni and Pt SACs show good selectivity toward the production of CH₃OH, while Os and Ru prefer the reduction of CO₂ to CH₄.

Notably, in several recent studies of non-noble transition metals, Ni SACs exhibit very good CO₂RR activity. Yang et al.^[106] pyrolyzed a mixture of amino acid (with or without sulfur), melamine and nickel acetate under an argon atmosphere. From the TEM image in **Figure 14a**, it can be seen that the resulting sample exhibited a smooth surface, with single Ni atoms (white spots) dispersed throughout the material. Results from XPS studies suggested the formation of Ni-N and Ni-S, at the respective Ni concentration of 4 wt% and 2.5 wt% in N and S co-doped carbon (NSG). Furthermore, XAS study showed that the valence state of Ni was +1, consistent with results from EPR measurements, an oxidation state favored for CO₂RR. XANES measurements suggested the formation of MN₄ structures in D_{4h} symmetry (**Figure 14b**),

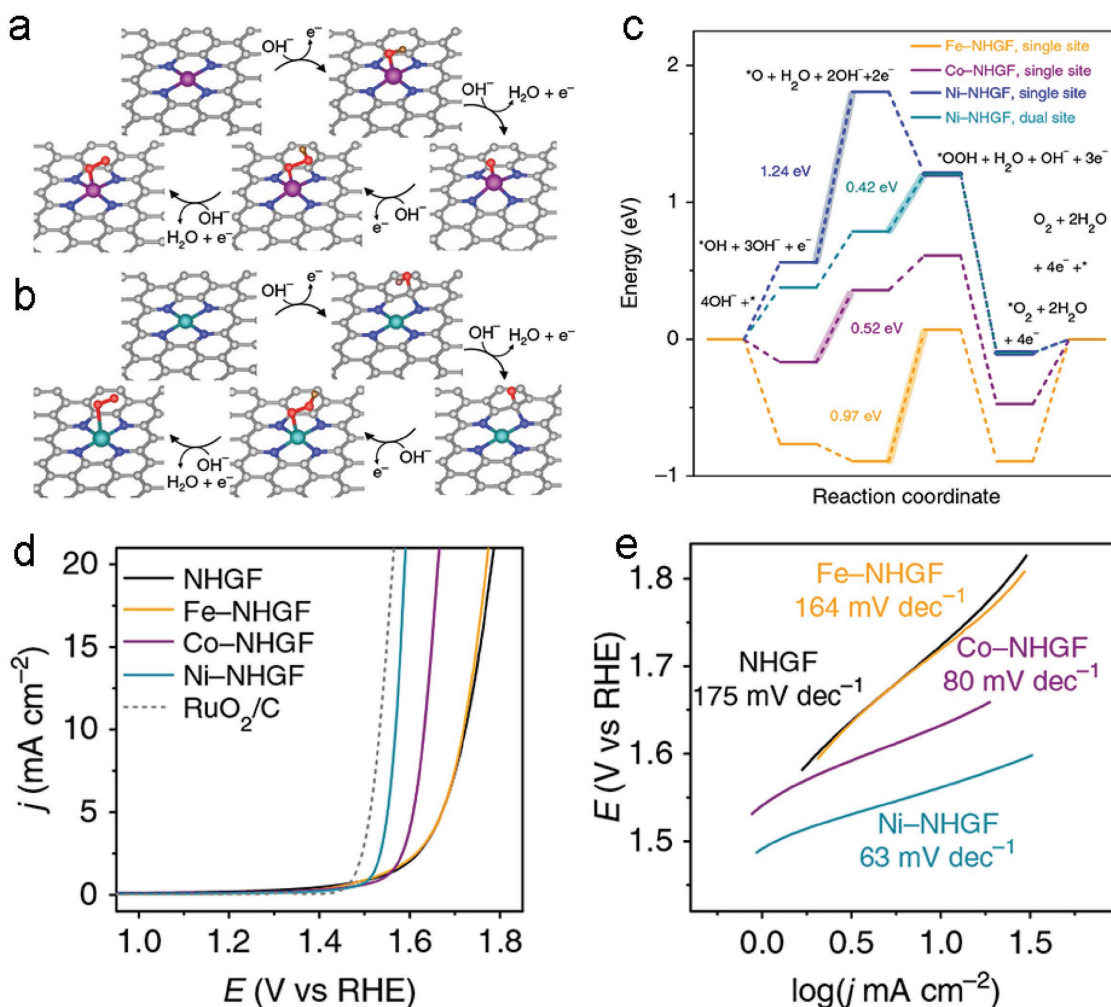


Figure 12. a,b) Proposed OER mechanism of MN₄C₄ with the intermediates adsorbed on the single site (M = Fe or Co) (a) and dual site (M = Ni) (b). c) Free energy diagram at 1.23 V for OER at M-NHGF with MN₄C₄ moieties. d) OER activity evaluated by LSV (with iR correction) in 1 M KOH at the potential scan rate of 5 mV s⁻¹ for M-NG, NG, and commercial RuO₂/C. e) Corresponding Tafel plots of the catalysts. Reproduced with permission.^[105] Copyright 2018, Macmillan Publishers Limited.

consistent with results from EXAFS studies, where the peaks for Ni–N (1.45 Å) and Ni–S (1.81 Å) bonds were clearly defined, whereas the Ni–Ni peak at 2.15 Å was not observed (Figure 14c). In electrochemical measurements (Figure 14d), one can see that the N-doped carbon alone exhibited only negligible CO₂RR activity, which was slightly improved with the deposition of Ni nanoparticles, and marked improvement was observed with NSG-supported Ni SACs in the reduction of CO₂ to CO. The Ni SACs exhibited a Faradaic efficiency up to 97%. DFT calculations showed that the Ni(I) site was most likely responsible for the CO₂RR activity. In another study,^[108] Zhao et al. pyrolyzed a ZIF-8 MOF loaded with Ni²⁺ ions. The nickel valence state of the resulting sample was identified to be between Ni(0) to Ni(II), in the form of NiN₃. Electrochemical measurements showed that the obtained Ni SAC exhibited a much better CO₂RR performance than Ni nanoparticles. In fact, the Faradaic efficiency of CO₂RR to CO can reach 71.9%. Several other studies also showed that Ni SACs of Ni-NC were effective in reducing CO₂ to CO.^[75,89]

SACs based on a “host–guest” structure have also been used for CO₂RR electrocatalysis. For instance, Zhang et al.^[219] deposited cobalt phthalocyanine (CoPc, 6 wt%) onto CNT via π - π interactions (Figure 15a), and the electrocatalytic performance toward CO₂RR was examined by CV measurements, in comparison with other catalysts such as Pc/CNT, CoPc/rGO and CoPc/CB (Figure 15b). One can see that Co single atoms coordinated in Pc played a significant role in the catalytic reaction, and among the various types of carbon supports, CNTs-supported catalysts showed the best activity, likely due to the highest degree of graphitization of CNTs which facilitated π - π interactions with CoPc and highest electrical conductivity.^[220] Furthermore, the selectivity of the catalysts were compared at -0.59 V, and CoPc/CNT showed the highest Faradaic efficiency (FE) for CO but the lowest for H₂ (Figure 15c). Interestingly, when the CoPc phenyl rings were further functionalized with CN groups (CoPc-CN), the resulted hybrid catalyst, CoPc-CN/CNT (Figure 15d inset), showed an even higher reduction current density and better selectivity than CoPc/CNT in the

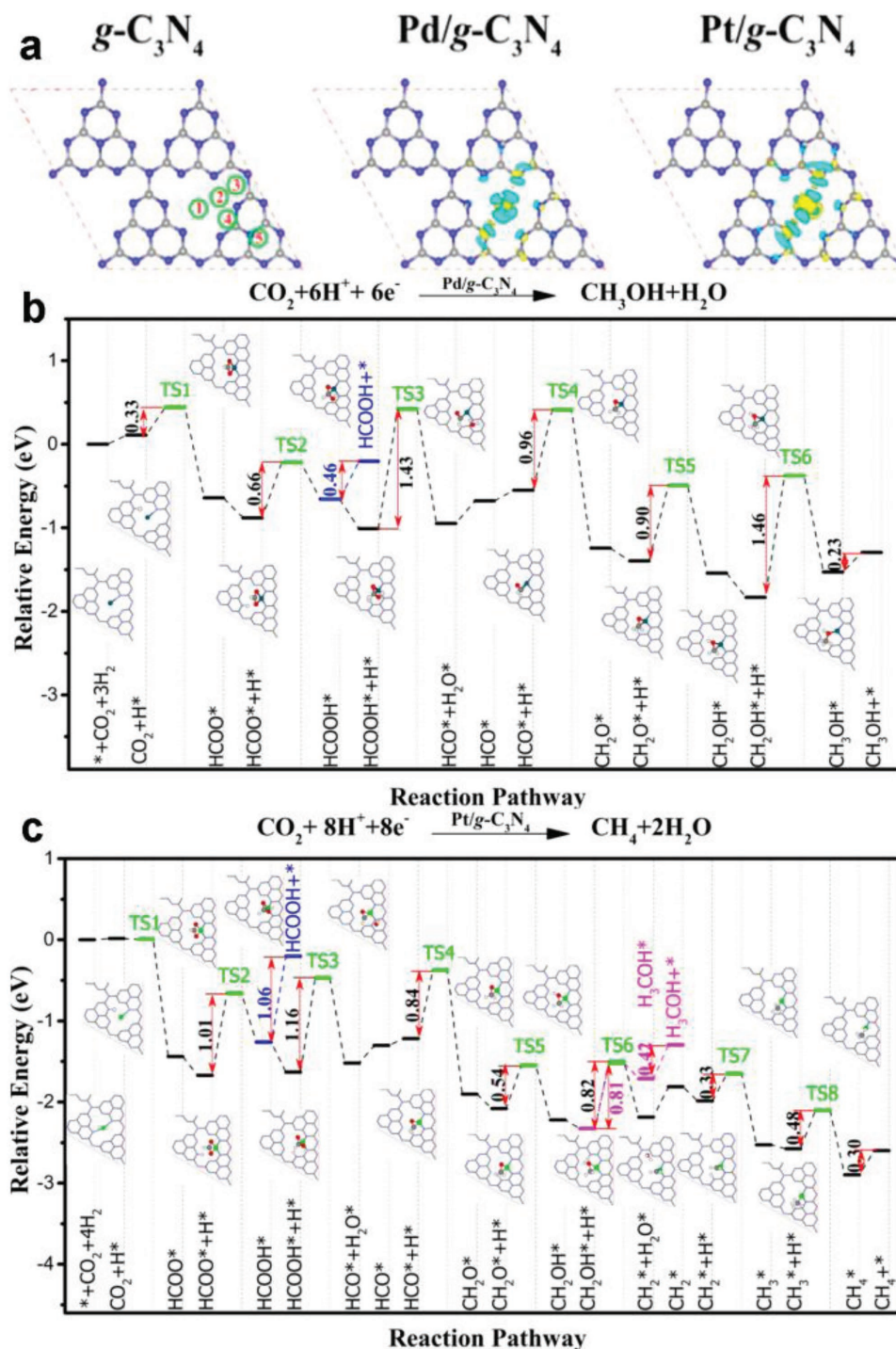


Figure 13. a) Optimized structure of pristine $g\text{-C}_3\text{N}_4$, $\text{Pd}/\text{C}_3\text{N}_4$ and $\text{Pt}/\text{C}_3\text{N}_4$. The yellow and blue in $\text{Pd}/\text{C}_3\text{N}_4$ and $\text{Pt}/\text{C}_3\text{N}_4$ indicate charge accumulation and charge depletion with an isovalue of $0.005\text{e}/\text{\AA}^3$. b,c) Reaction pathways of CO_2 reduction catalyzed by $\text{Pd}/\text{C}_3\text{N}_4$ (b) and $\text{Pt}/\text{C}_3\text{N}_4$ (c) under standard conditions: Pt, green; C, grey; O, red; and H, white. Reproduced with permission.^[109] Copyright 2016, American Chemical Society.

reduction of CO_2 to CO at the same potential (Figure 15d). This enhancement by CN substitution was attributed to the electron-withdrawing effect.^[221] Note that in previous studies,^[222,223] significant CO_2RR activity has also been observed with homogeneous molecular catalysts that featured a MN_4 structure ($M = \text{Fe}$ or Co).

3.5. Multifunctional Catalysts

In the above discussion, one may notice that some catalysts are actually active in multiple reactions. For instance, Co-NC SACs have been employed as effective catalysts toward HER, OER and ORR in separate studies,^[91,97,105] and Ni-NC SACs show apparent

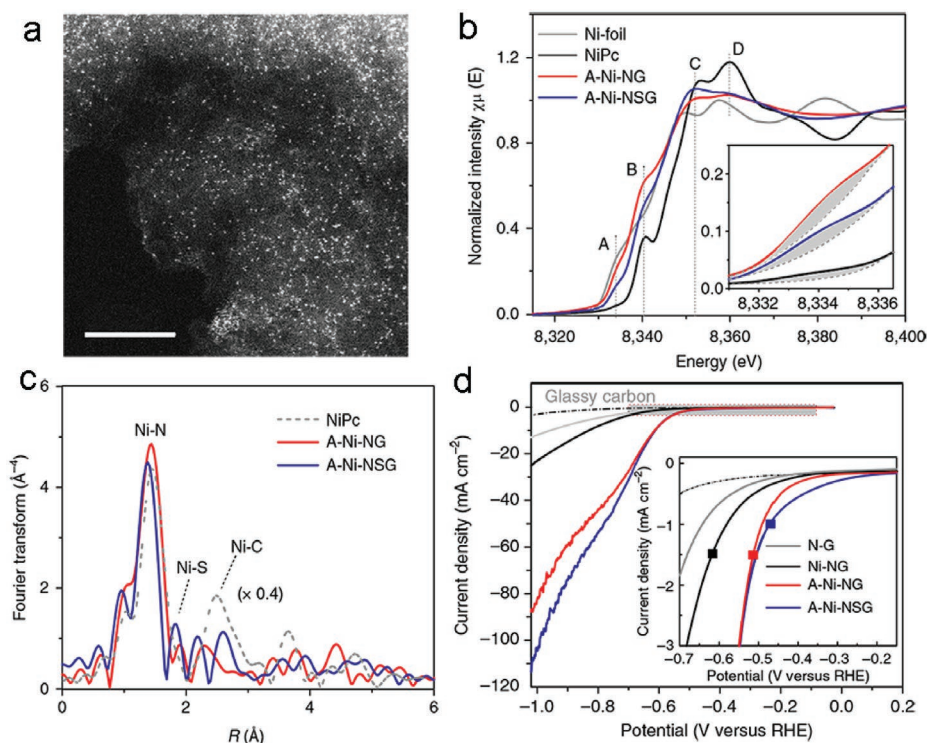


Figure 14. a) HAADF-STEM image of Ni-NG; scale bar 5 nm. b) Ni K-edge XANES spectra of Ni-NG, Ni-NSG and NiPc, where peak A represents $1s \rightarrow 3d$ transition, peak B represents $1s \rightarrow 4p_z$ transition, C and D represent $1s \rightarrow 4p_{x,y}$ transitions and multiple scattering processes, respectively (inset shows the expanded pre-edge region). c) Fourier-transformed EXAFS spectra in which the NiPc spectrum has been reduced in size. d) LSV curves acquired in a CO_2 -saturated 0.5 M KHCO_3 solution on a rotating disc electrode at a rotation speed of 1600 rpm and potential scan rate of 5 mV s^{-1} . Catalyst loading 0.1 mg cm^{-2} . The inset highlights the LSV curves in the potential range of -0.1 to -0.7 V versus RHE. The dots on the curves show the specific CO formation current of $10 \text{ mA mg}_{\text{catalyst}}^{-1}$. Reproduced with permission.^[106] Copyright 2018, Macmillan Publishers Limited.

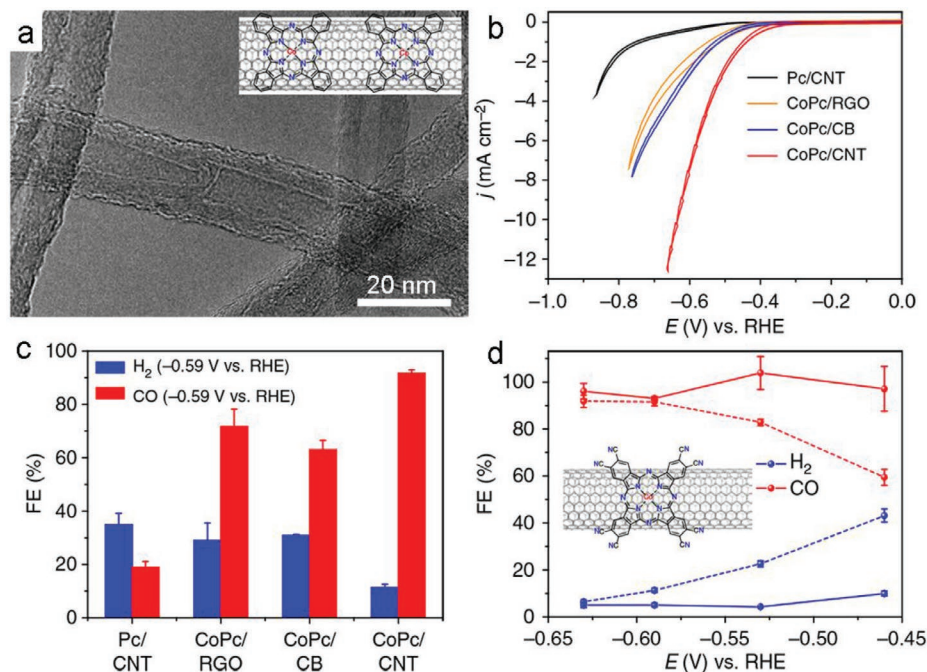


Figure 15. a) TEM image of CoPc/CNT (6%). Inset is the schematic structure of the CoPc/CNT hybrid. b) CO_2 reduction reaction tested by CV measurements in 0.1 M KHCO_3 using Pc/CNT, CoPc/RGO, CoPc/CB, and CoPc/CNT as the electrocatalysts. c) Faradaic efficiencies of CO_2 reduction products (CO and H_2) catalyzed by various electrocatalysts at -0.59 V versus RHE. d) Faradaic efficiencies of CO_2 reduction products at different potentials for CoPc/CNT (dash lines) and CoPc-CN/CNT (solid lines). Inset is a schematic of the hybrid structure. Reproduced with permission.^[219] Published under CC-BY 4.0 license. Copyright 2016, the Authors.

electrocatalytic activity toward CO₂RR, HER and OER.^[105–108] This suggests that some of these SACs may act as bifunctional or even multifunctional catalysts, a unique feature that is important for rechargeable batteries. For instance, Cu SACs supported on GO/MOF hybrids^[83] exhibit low overpotentials and high current densities for ORR, OER and HER, as compared to that without GO, because of the porous scaffold for enhanced mass transfer, efficient charge-transport, and synergistic interactions between GO and MOF. Zheng et al.^[126] reported bifunctional activity of P and Co co-doped rGO toward ORR and OER, and the electrocatalytic activity of the resulting Co SACs was accounted for by the formation of rGO structural defects after co-doping and modification of the charge and spin density, although there was no explicit experimental evidence to substantiate the argument. In another study,^[224] Du and coworkers carried out ab initio studies to understand the interaction between metal dopant and graphene matrix, and the effect on the HER and OER performances. Generally, the M-C moieties are assumed as the active sites for the adsorption of reaction intermediates. The possible doping structures are schematically illustrated in Figure 16a, and calculations of different Ni sites showed that the interaction with hydrogen was weakened by increasing the Ni coordination number. Figure 16b shows the volcano plot of a variety of transition metals, including Mn, Fe, Co, Cu, and Pd, at low coordination numbers (1 to 2). The structures located around the peak, such as Ni@1-zigzag, Fe@1-armchair, and Co@1-zigzag, are expected to possess a best HER performance. Figure 16c depicts the volcano plots of theoretical overpotentials using the O* and OH* binding energy as the reaction descriptors.^[225] Based on the plots, one can clearly see that Ni@4 has the lowest overpotential of 0.35 V among the structures and is close to the peak of OER at +0.24 V, thus is expected to show the best OER activity. Pd@4 and Pd@2-armchair are identified as the next best samples. These results suggest that selection of metal SACs can be approached by optimizing the coordination number of the MC_x moieties.

More complicated structures involving SACs have also been reported. For instance, in one study,^[136] Fe SACs were embedded into a nitrogen-doped carbon matrix in the form of FeN₄, and a second Pt SAC was then loaded onto the sample surface via a Pt-O₂-Fe-N₄ configuration, as confirmed by Fourier-transformed EXAFS measurements (Figure 17a,b). Figure 17c shows two possible structures of the proposed moiety. The resulting catalyst, Pt₁@Fe-NC SAC, exhibited much enhanced activity toward ORR, HER, and OER, as compared to Fe-NC SAC. Specifically, based on LSV measurements (Figure 17d), the ORR E_{onset} was identified at +0.93 V and E_{1/2} at +0.80 V for Pt₁@Fe-NC in 0.5 M H₂SO₄, a performance somewhat better than that of Fe-NC SAC. In addition, LSV measurements for up to 10000 potential cycles (Figure 17e) showed that E_{1/2} of Pt₁@Fe-NC shifted negatively only by 12 mV, and a much larger negative shift (36 mV) was observed for Fe-NC SAC. The durability of the catalysts was also tested in an acidic PEMFC for 50 h, and the Pt₁@Fe-NC catalyst was found to decay slower than Fe-NC SAC (Figure 17f). This suggests that the introduction of Pt SAC into the catalyst markedly improved the durability. As for HER, Pt₁@Fe-NC showed apparent activity in both acidic and basic electrolytes (Figure 17g,h). The η₁₀ value was found to decrease from -130 mV to -60 mV in 0.5 M H₂SO₄ and from -165 mV to -110 mV in 1.0 M KOH after the introduction of

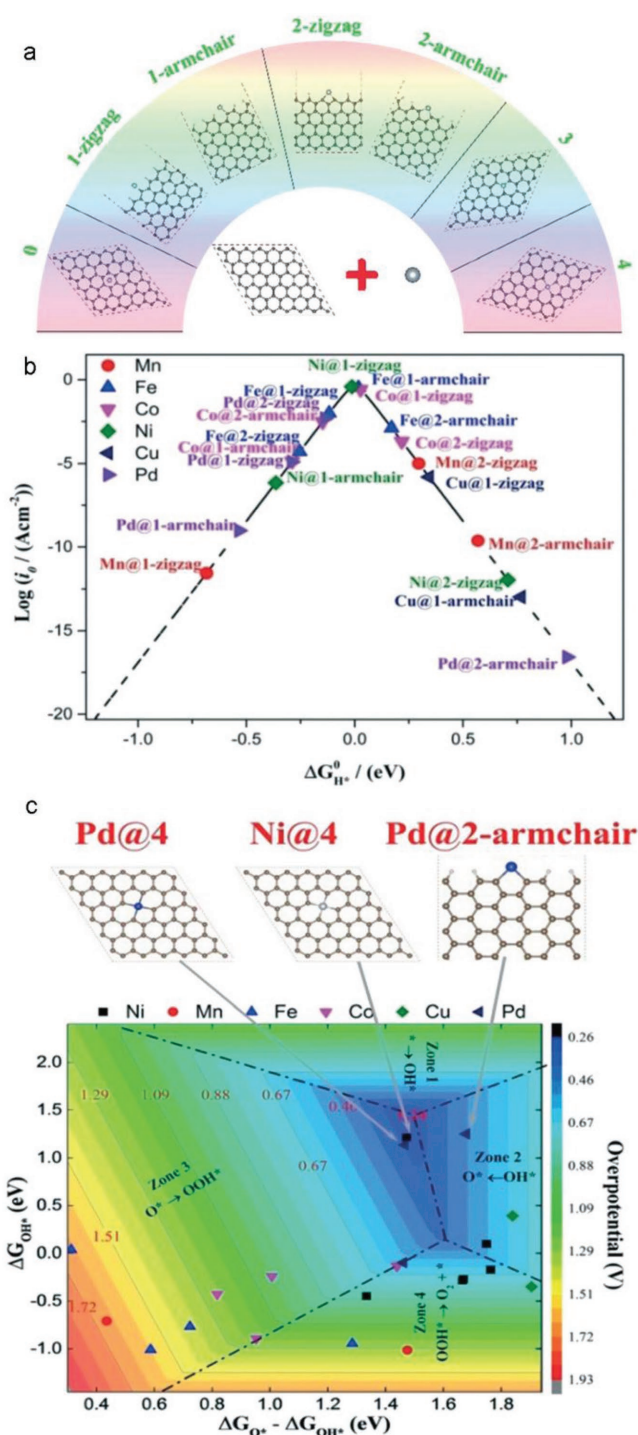


Figure 16. a) M-G (M = Mn, Fe, Co, Ni, Cu and Pd) composite models with different coordination numbers (C sites) of the Ni sites: carbon, brown; hydrogen, white; and nickel, grey. b) HER volcano curve of exchange current (i_0) as a function of the Gibbs free energy of hydrogen adsorption (ΔG_{H^*}) on various low coordinated transition metals. c) Theoretical OER overpotential volcano plot with O* and OH* binding energy as descriptors to compare the theoretical activity of M-G composite catalysts. Reproduced with permission.^[224] Copyright 2017, Royal Society of Chemistry.

Pt SAC. The enhancement was attributed to the formation of a heteroatom pair of Pt-O₂-Fe that was favorable for the cleavage

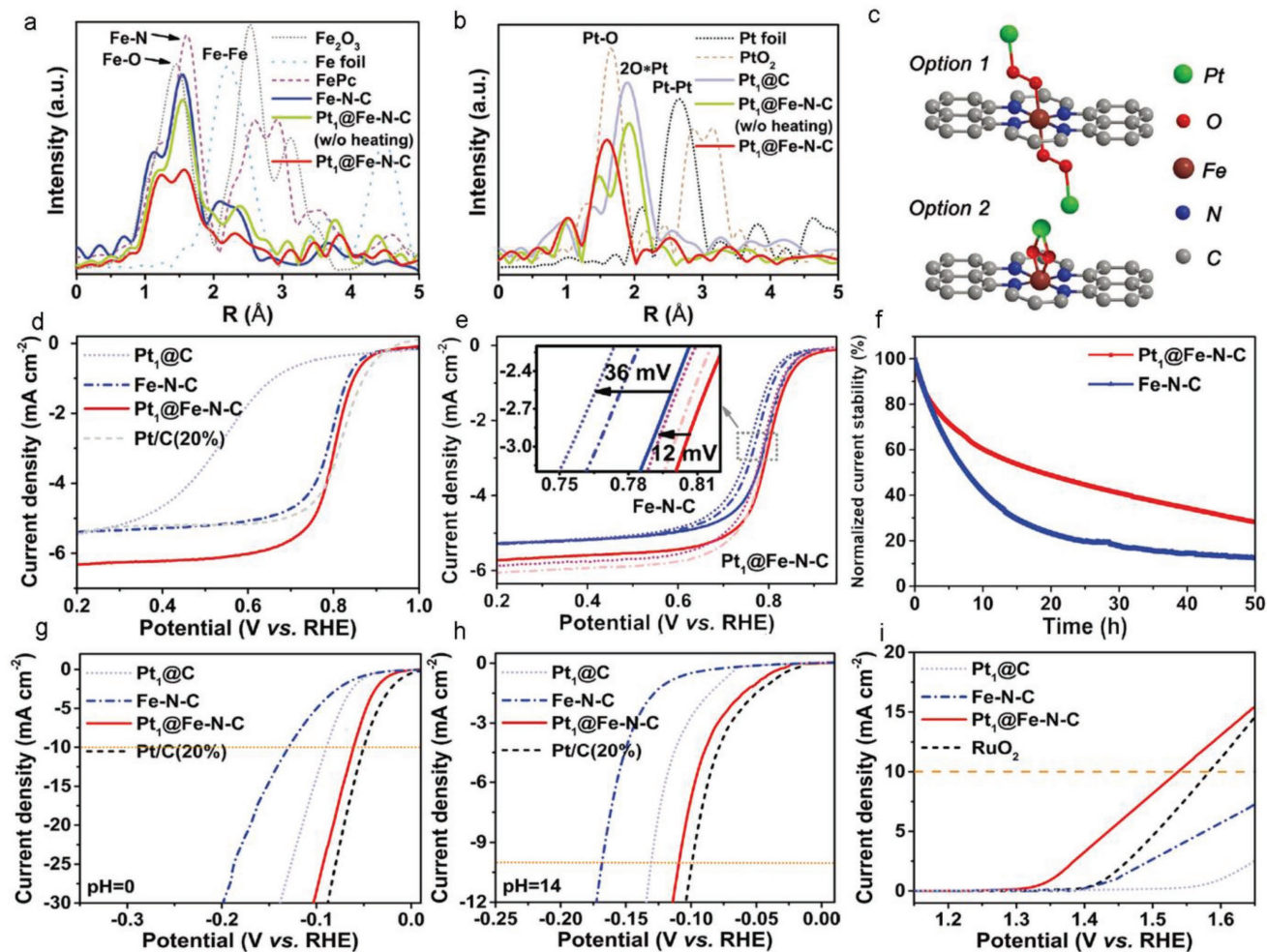


Figure 17. a, b) k^3 -Weighted, Fourier-transformed EXAFS data of Fe (a) and Pt (b) in a series of samples, including Pt₁@Fe-N-C. c) Two proposed structures of Pt-O₂-Fe-N-C moieties. d) LSV curves of various catalyst samples acquired by RRDE measurements in O₂-saturated 0.5 M H₂SO₄. e) LSV curves of (red curves) Pt₁@Fe-N-C and (blue curves) Fe-N-C in the first (solid curves), 5000th (dashed-dotted curves) and 10 000th potential cycles (dotted curves) in an air-saturated electrolyte. f) Normalized current density of Fe-N-C and Pt₁@Fe-N-C in a fuel cell during continuous operation for 50 h at 0.5 V with 80 °C H₂/O₂, 100% RH. g, h) HER polarization curves of the various catalysts in 0.5 M H₂SO₄ (g) and 1.0 M KOH (h) electrolytes. i) OER polarization curves of the catalysts in 0.1 M KOH. Reproduced with permission.^[136] Copyright 2017, Wiley-VCH.

of H–OH bond and to the Pt-O₂- linkage that might enhance water desorption due to electronic and steric effects on the FeN₄ moiety.^[226,227] For OER electrocatalysis, LSV measurements (Figure 17i) showed that to reach the current density of 10 mA cm⁻², the electrode potential (E_{10}) was about +1.54 V for Pt₁@FeSA-NC, markedly lower than those for Fe-N-C and Pt/C and even better than that of state-of-the-art RuO₂ catalysts ($E_{10} \approx +1.58$ V).

Notably, the bifunctional electrocatalysts for ORR and OER can be applied to rechargeable metal-air batteries.^[228–230] For instance, Chen et al.^[231] examined the performance of a rechargeable Zn-air battery using FeN_x species on N and S co-doped carbon layers coated on CNT (denoted as S,N-Fe/N/C-CNT, Figure 18a) as the electrode materials. The bifunctional electrocatalytic activity toward ORR and OER was first quantified by voltammetric measurements, where the oxygen electrode potential, $\Delta E = \eta_{10, \text{OER}} - E_{1/2, \text{ORR}}$, for S,N-Fe/N/C-CNT was only 0.75 V (Figure 18b), much lower than that of Pt/C (1.12 V) and other catalysts in recent literatures.^[213,232–234] Although the performance

was a combined contribution of various components in the catalysts, the FeN_x species were thought to play a major role. The catalyst was then integrated into a Zn-air battery with S,N-Fe/N/C-CNT as the cathode and a Zn plate anode (Figure 18c). From the charge–discharge polarization curves (Figure 18d), one can see that the open circuit voltage (1.35 V) was higher than that with commercial Pt/C as the cathode, indicating enhanced performance of the device. When the discharge polarization curves were converted into power density plots (Figure 18e), it was found that the power density of the S,N-Fe/N/C-CNT battery was as high as 102.7 mW cm⁻²; and there was no obvious voltage change over 100 cycles (Figure 18f), suggesting excellent long-term stability of the catalyst in Zn-air batteries.

4. Summaries and Perspectives

Single metal atoms supported on carbon-based materials represent a new class of low-cost, high-efficiency electrocatalysts

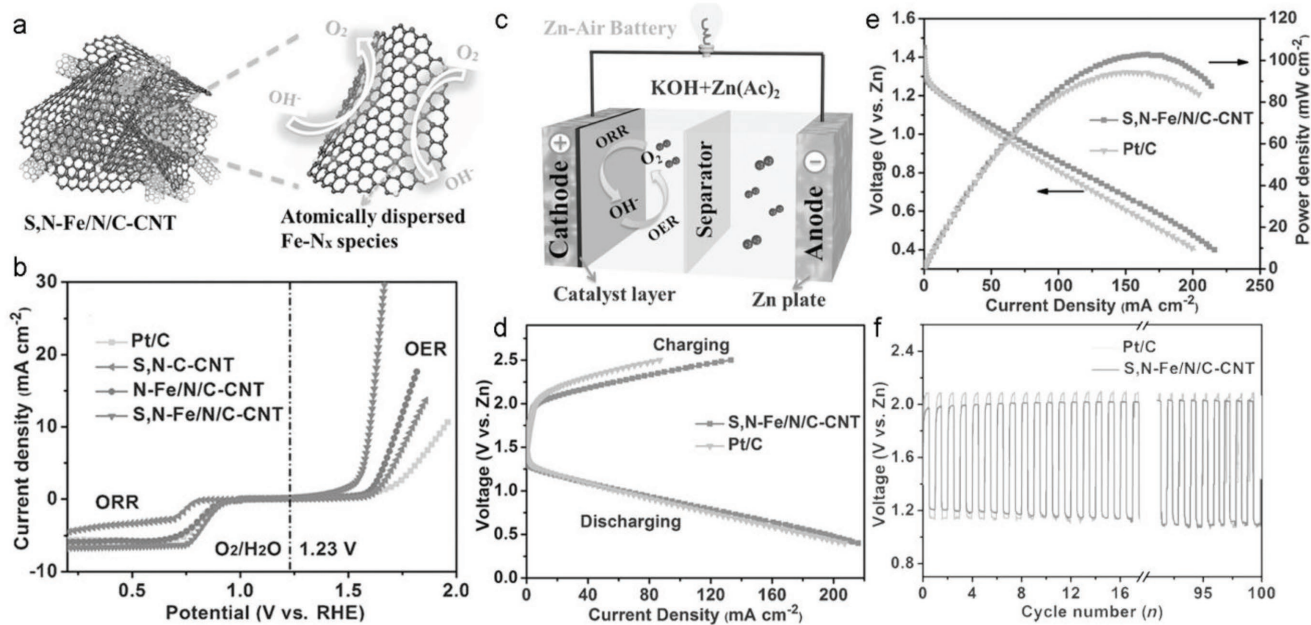


Figure 18. a) Schematic morphology of S,N-Fe/N/C-CNT and the atomic structure of Fe-N_x species in the carbon matrix. b) Overall polarization curves of S,N-Fe/N/C-CNT in ORR and OER in 0.1 M KOH, in comparison with other catalysts. c) Schematic illustration of a rechargeable Zn-air battery with the S,N-Fe/N/C-CNT catalyst as the cathode and a Zn plate as the anode. d) Charge and discharge polarization curves of the Zn-air battery in (c). e) Discharge polarization curves and corresponding power density plots. f) Charge-discharge cycling performance at a constant charge-discharge current density of 5 mA cm⁻² of the Zn-air battery in (c) with Pt/C as the cathode catalysts. Reproduced with permission.^[231] Copyright 2017, Wiley-VCH.

in important electrochemical reactions that are of fundamental and technological significance in electrochemical energy conversion and storage, such as HER, ORR, OER and CO₂RR. In this review, leading strategies for the synthesis of SACs are first summarized, such as pyrolysis, wet-chemistry routes, physical and chemical vapor deposition, electrochemical deposition, and ball milling. In the resulting samples, SACs primarily involve metal atoms bound to nonmetal atoms such as C, N, O, S, and P of the carbon supporting matrix through covalent bonds or coordination bonds, and the maximal metal–matrix interfacial interaction leads to the manipulation of the electronic structures of the materials, and emergence of additional active sites. This is a key attribute that plays an important role in regulating the reaction dynamics and eventual electrocatalytic activity, and distinguishes SACs from conventional nanoparticle catalysts, in that new reaction pathways and electron-transfer dynamics may emerge.

Despite the progress, challenges remain. For instance, the loading of active materials in SACs is generally minimal, leading to the production of only a low current density unfit for practical applications. Yet at increasing loadings one may inevitably face the issues of migration and agglomeration of metal atoms to form nanoparticles. Thus, a delicate balance needs to be struck between SAC loading and electrocatalytic activity. This may take advantage of theoretical modeling and simulations for SAC design and engineering and development of effective synthetic chemistry, such that SACs at high metal loadings and uniform coordination structures can be produced. As demonstrated in the cited examples in this review, an integration of theory and experiment is critical in advancing our understanding of the reaction mechanism,

and developing a fundamental framework within which further engineering and optimization of the catalysts can be achieved. In addition, given the experimental challenges encountered in SAC synthesis, for instance, when SACs are extended to non-carbon supporting matrices, sometimes theoretical studies are anticipated to play a leading role. This necessitates the development of effective computational methods and tools.

Furthermore, diverse metal-nonmetal bonding interactions have been formed in organometallic chemistry and played a critical role in a wide range of catalytic reactions. The fundamental insights have been exploited for the deliberate functionalization of metal nanoparticles. For instance, for conjugated metal–ligand interfacial bonding interactions, intraparticle charge delocalization occurs between the particle-bound functional moieties.^[235] Such a delicate control of the nanoparticle electronic properties have been exploited for the manipulation of nanoparticle catalysts in a range of electrochemical reactions. For metal SACs, this interfacial interaction is anticipated to be even more pronounced, leading to an ever increasing level of control of the electrocatalytic activity. To this end, drastic progress has to be made on both the synthetic front and structural characterizations. This will be a focus in future research.

Acknowledgements

Y.P. and B.Z.L. contributed equally to this work. The authors thank the National Science Foundation (CHE-1710408 and DMR-1409396) for partial support of the work. We also thank the anonymous reviewers for their helpful comments and critiques.

Conflict of Interest

The authors declare no conflict of interest.

Keywords

CO₂ reduction reaction, hydrogen evolution reaction, oxygen evolution reaction, oxygen reduction reaction, single atom catalysts

Received: March 28, 2018

Revised: May 30, 2018

Published online:

- [1] G. Li, Z. Tang, *Nanoscale* **2014**, *6*, 3995.
- [2] B. Wu, N. Zheng, *Nano Today* **2013**, *8*, 168.
- [3] B. Wu, Y. Kuang, X. Zhang, J. Chen, *Nano Today* **2011**, *6*, 75.
- [4] X. Liu, J. Iocozzia, Y. Wang, X. Cui, Y. Chen, S. Zhao, Z. Li, Z. Lin, *Energy Environ. Sci.* **2017**, *10*, 402.
- [5] J. Fang, B. Zhang, Q. Yao, Y. Yang, J. Xie, N. Yan, *Coordin. Chem. Rev.* **2016**, *322*, 1.
- [6] H. L. Liu, F. Nosheen, X. Wang, *Chem. Soc. Rev.* **2015**, *44*, 3056.
- [7] M. H. Shao, Q. W. Chang, J. P. Dodelet, R. Chenitz, *Chem. Rev.* **2016**, *116*, 3594.
- [8] K. D. Gilroy, A. Ruditskiy, H. C. Peng, D. Qin, Y. Xia, *Chem. Rev.* **2016**, *116*, 10414.
- [9] Z. Fan, H. Zhang, *Acc. Chem. Res.* **2016**, *49*, 2841.
- [10] B. E. Hayden, *Acc. Chem. Res.* **2013**, *46*, 1858.
- [11] W. Chen, S. W. Chen, *Angew. Chem., Int. Ed.* **2009**, *48*, 4386.
- [12] F. J. Perez-Alonso, D. N. McCarthy, A. Nierhoff, P. Hernandez-Fernandez, C. Streb, I. E. L. Stephens, J. H. Nielsen, I. Chorkendorff, *Angew. Chem., Int. Ed.* **2012**, *51*, 4641.
- [13] D. F. Gao, H. Zhou, J. Wang, S. Miao, F. Yang, G. X. Wang, J. G. Wang, X. H. Bao, *J. Am. Chem. Soc.* **2015**, *137*, 4288.
- [14] N. S. Porter, H. Wu, Z. W. Quan, J. Y. Fang, *Acc. Chem. Res.* **2013**, *46*, 1867.
- [15] J. B. Wu, A. Gross, H. Yang, *Nano Lett.* **2011**, *11*, 798.
- [16] J. Y. Chen, B. Lim, E. P. Lee, Y. N. Xia, *Nano Today* **2009**, *4*, 81.
- [17] Y. J. Kang, P. D. Yang, N. M. Markovic, V. R. Stamenkovic, *Nano Today* **2016**, *11*, 587.
- [18] Z. W. Quan, Y. X. Wang, J. Y. Fang, *Acc. Chem. Res.* **2013**, *46*, 191.
- [19] M. S. Jin, H. Zhang, Z. X. Xie, Y. N. Xia, *Angew. Chem., Int. Ed.* **2011**, *50*, 7850.
- [20] L. D. Li, Y. Peng, Y. H. Yue, Y. Hu, X. Liang, P. G. Yin, L. Guo, *Chem. Commun.* **2015**, *51*, 11591.
- [21] N. Tian, Z. Y. Zhou, S. G. Sun, Y. Ding, Z. L. Wang, *Science* **2007**, *316*, 732.
- [22] T. Sheng, Y. F. Xu, Y. X. Jiang, L. Huang, N. Tian, Z. Y. Zhou, I. Broadwell, S. G. Sun, *Acc. Chem. Res.* **2016**, *49*, 2569.
- [23] C. H. Cui, S. H. Yu, *Acc. Chem. Res.* **2013**, *46*, 1427.
- [24] Y. J. Wang, N. N. Zhao, B. Z. Fang, H. Li, X. T. T. Bi, H. J. Wang, *Chem. Rev.* **2015**, *115*, 3433.
- [25] D. M. Alonso, S. G. Wettstein, J. A. Dumesic, *Chem. Soc. Rev.* **2012**, *41*, 8075.
- [26] C. Chen, Y. J. Kang, Z. Y. Huo, Z. W. Zhu, W. Y. Huang, H. L. L. Xin, J. D. Snyder, D. G. Li, J. A. Herron, M. Mavrikakis, M. F. Chi, K. L. More, Y. D. Li, N. M. Markovic, G. A. Somorjai, P. D. Yang, V. R. Stamenkovic, *Science* **2014**, *343*, 1339.
- [27] X. Q. Huang, Z. P. Zhao, L. Cao, Y. Chen, E. B. Zhu, Z. Y. Lin, M. F. Li, A. M. Yan, A. Zettl, Y. M. Wang, X. F. Duan, T. Mueller, Y. Huang, *Science* **2015**, *348*, 1230.
- [28] B. Lim, M. J. Jiang, P. H. C. Camargo, E. C. Cho, J. Tao, X. M. Lu, Y. M. Zhu, Y. N. Xia, *Science* **2009**, *324*, 1302.
- [29] K. Parvez, S. B. Yang, Y. Hernandez, A. Winter, A. Turchanin, X. L. Feng, K. Mullen, *ACS Nano* **2012**, *6*, 9541.
- [30] D. K. Perivoliotis, N. Tagmatarchis, *Carbon* **2017**, *118*, 493.
- [31] M. Zhou, H. L. Wang, S. J. Guo, *Chem. Soc. Rev.* **2016**, *45*, 1273.
- [32] D. Higgins, P. Zamani, A. P. Yu, Z. W. Chen, *Energy Environ. Sci.* **2016**, *9*, 357.
- [33] Q. Li, N. Mahmood, J. H. Zhu, Y. L. Hou, S. H. Sun, *Nano Today* **2014**, *9*, 668.
- [34] Q. R. Shi, Y. Cha, Y. Song, J. I. Lee, C. Z. Zhu, X. Y. Li, M. K. Song, D. Du, Y. H. Lin, *Nanoscale* **2016**, *8*, 15414.
- [35] F. Bonaccorso, L. Colombo, G. H. Yu, M. Stoller, V. Tozzini, A. C. Ferrari, R. S. Ruoff, V. Pellegrini, *Science* **2015**, *347*, 1246501.
- [36] X. F. Yang, A. Q. Wang, B. T. Qiao, J. Li, J. Y. Liu, T. Zhang, *Acc. Chem. Res.* **2013**, *46*, 1740.
- [37] J. Cordon, G. Jimenez-Oses, J. M. Lopez-de-Luzuriaga, M. Monge, *Nat. Commun.* **2017**, *8*, 1657.
- [38] J. Li, X. Li, H. J. Zhai, L. S. Wang, *Science* **2003**, *299*, 864.
- [39] M. Valden, X. Lai, D. W. Goodman, *Science* **1998**, *281*, 1647.
- [40] A. Behr, P. Neubert, *Applied Homogeneous Catalysis*, Wiley-VCH, Weinheim, Germany **2012**.
- [41] B. Han, R. Lang, B. T. Qiao, A. Q. Wang, T. Zhang, *Chin. J. Catal.* **2017**, *38*, 1498.
- [42] C. Lecuyer, F. Quignard, A. Choplin, D. Olivier, J. M. Basset, *Angew. Chem., Int. Ed.* **1991**, *30*, 1660.
- [43] V. Vidal, A. Theolier, J. ThivolleCazat, J. M. Basset, J. Corker, *J. Am. Chem. Soc.* **1996**, *118*, 4595.
- [44] B. T. Qiao, A. Q. Wang, X. F. Yang, L. F. Allard, Z. Jiang, Y. T. Cui, J. Y. Liu, J. Li, T. Zhang, *Nat. Chem.* **2011**, *3*, 634.
- [45] X. K. Gu, B. T. Qiao, C. Q. Huang, W. C. Ding, K. J. Sun, E. S. Zhan, T. Zhang, J. Y. Liu, W. X. Li, *ACS Catal.* **2014**, *4*, 3886.
- [46] C. L. Wang, X. K. Gu, H. Yan, Y. Lin, J. J. Li, D. D. Liu, W. X. Li, J. L. Lu, *ACS Catal.* **2017**, *7*, 887.
- [47] Y. R. Li, Z. W. Wang, T. Xia, H. X. Ju, K. Zhang, R. Long, Q. Xu, C. M. Wang, L. Song, J. F. Zhu, J. Jiang, Y. J. Xiong, *Adv. Mater.* **2016**, *28*, 6959.
- [48] Y. T. Shi, C. Y. Zhao, H. S. Wei, J. H. Guo, S. X. Liang, A. Q. Wang, T. Zhang, J. Y. Liu, T. L. Ma, *Adv. Mater.* **2014**, *26*, 8147.
- [49] S. E. J. Hackett, R. M. Brydson, M. H. Gass, I. Harvey, A. D. Newman, K. Wilson, A. F. Lee, *Angew. Chem., Int. Ed.* **2007**, *46*, 8593.
- [50] R. Lang, T. Li, D. Matsumura, S. Miao, Y. Ren, Y. T. Cui, Y. Tan, B. Qiao, L. Li, A. Wang, X. Wang, T. Zhang, *Angew. Chem., Int. Ed.* **2016**, *55*, 16054.
- [51] S. Yang, J. Kim, Y. J. Tak, A. Soon, H. Lee, *Angew. Chem., Int. Ed.* **2016**, *55*, 2058.
- [52] B. Zhang, H. Asakura, J. Zhang, J. G. Zhang, S. De, N. Yan, *Angew. Chem., Int. Ed.* **2016**, *55*, 8319.
- [53] J. Lin, B. T. Qiao, N. Li, L. Li, X. C. Sun, J. Y. Liu, X. D. Wang, T. Zhang, *Chem. Commun.* **2015**, *51*, 7911.
- [54] J. X. Liang, J. Lin, X. F. Yang, A. Q. Wang, B. T. Qiao, J. Y. Liu, T. Zhang, J. Li, *J. Phys. Chem. C* **2014**, *118*, 21945.
- [55] J. Lin, A. Q. Wang, B. T. Qiao, X. Y. Liu, X. F. Yang, X. D. Wang, J. X. Liang, J. X. Li, J. Y. Liu, T. Zhang, *J. Am. Chem. Soc.* **2013**, *135*, 15314.
- [56] J. C. Matsubu, V. N. Yang, P. Christopher, *J. Am. Chem. Soc.* **2015**, *137*, 3076.
- [57] H. Yan, H. Cheng, H. Yi, Y. Lin, T. Yao, C. L. Wang, J. J. Li, S. Q. Wei, J. L. Lu, *J. Am. Chem. Soc.* **2015**, *137*, 10484.
- [58] F. Dvorak, M. Farnesi Camellone, A. Tovt, N. D. Tran, F. R. Negreiros, M. Vorokhta, T. Skala, I. Matolinova, J. Myslivecek, V. Matolin, S. Fabris, *Nat. Commun.* **2016**, *7*, 10801.
- [59] L. B. Wang, W. B. Zhang, S. P. Wang, Z. H. Gao, Z. H. Luo, X. Wang, R. Zeng, A. W. Li, H. L. Li, M. L. Wang, X. S. Zheng, J. F. Zhu, W. H. Zhang, C. Ma, R. Si, J. Zeng, *Nat. Commun.* **2016**, *7*, 14036.

- [60] H. S. Wei, X. Y. Liu, A. Q. Wang, L. L. Zhang, B. T. Qiao, X. F. Yang, Y. Q. Huang, S. Miao, J. Y. Liu, T. Zhang, *Nat. Commun.* **2014**, *5*, 5634.
- [61] S. R. Zhang, L. Nguyen, J. X. Liang, J. J. Shan, J. Y. Liu, A. I. Frenkel, A. Patlolla, W. X. Huang, J. Li, F. Tao, *Nat. Commun.* **2015**, *6*, 7938.
- [62] J. Jones, H. F. Xiong, A. T. Delariva, E. J. Peterson, H. Pham, S. R. Challa, G. S. Qi, S. Oh, M. H. Wiebenga, X. I. P. Hernandez, Y. Wang, A. K. Datye, *Science* **2016**, *353*, 150.
- [63] W. E. Kaden, T. P. Wu, W. A. Kunkel, S. L. Anderson, *Science* **2009**, *326*, 826.
- [64] P. X. Liu, Y. Zhao, R. X. Qin, S. G. Mo, G. X. Chen, L. Gu, D. M. Chevrier, P. Zhang, Q. Guo, D. D. Zang, B. H. Wu, G. Fu, N. F. Zheng, *Science* **2016**, *352*, 797.
- [65] G. Zhao, H. Liu, J. Ye, *Nano Today* **2018**, *19*, 108.
- [66] H. Zhang, G. Liu, L. Shi, J. Ye, *Adv. Energy Mater.* **2018**, *8*, 1701343.
- [67] S. Liang, C. Hao, Y. Shi, *ChemCatChem* **2015**, *7*, 2559.
- [68] M. Yang, M. Flytzani-Stephanopoulos, *Catal Today* **2017**, *298*, 216.
- [69] L. Zhang, L. Han, H. Liu, X. Liu, J. Luo, *Angew. Chem., Int. Ed.* **2017**, *56*, 13694.
- [70] M. Xing, S. Guo, L. Guo, *Theor. Chem. Acc.* **2018**, *137*, 18.
- [71] J. Zhao, J.-X. Zhao, Q. Cai, *Phys. Chem. Chem. Phys.* **2018**, *20*, 9248.
- [72] M. Tavakkoli, N. Holmberg, R. Kronberg, H. Jiang, J. Sainio, E. I. Kauppinen, T. Kallio, K. Laasonen, *ACS Catal.* **2017**, *7*, 3121.
- [73] Y. Ding, A. Klyushin, X. Huang, T. Jones, D. Teschner, F. Girgsdies, T. Rodenas, R. Schlogl, S. Heumann, *Angew. Chem., Int. Ed.* **2018**, *57*, 3514.
- [74] B. Reuillard, J. Warnan, J. J. Leung, D. W. Wakerley, E. Reisner, *Angew. Chem., Int. Ed.* **2016**, *55*, 3952.
- [75] Y. Cheng, S. Zhao, B. Johannessen, J. P. Veder, M. Saunders, M. R. Rowles, M. Cheng, C. Liu, M. F. Chisholm, R. De Marco, H. M. Cheng, S. Z. Yang, S. P. Jiang, *Adv. Mater.* **2018**, *30*, 1706287.
- [76] P. D. Tran, A. Le Goff, J. Heidkamp, B. Jousseme, N. Guillet, S. Palacin, H. Dau, M. Fontecave, V. Artero, *Angew. Chem., Int. Ed.* **2011**, *50*, 1371.
- [77] N. C. Cheng, S. Stambula, D. Wang, M. N. Banis, J. Liu, A. Riese, B. W. Xiao, R. Y. Li, T. K. Sham, L. M. Liu, G. A. Botton, X. L. Sun, *Nat. Commun.* **2016**, *7*, 13638.
- [78] C. H. Choi, M. Kim, H. C. Kwon, S. J. Cho, S. Yun, H. T. Kim, K. J. J. Mayrhofer, H. Kim, M. Choi, *Nat. Commun.* **2016**, *7*, 10922.
- [79] C. Zhang, J. Sha, H. Fei, M. Liu, S. Yazdi, J. Zhang, Q. Zhong, X. Zou, N. Zhao, H. Yu, *ACS Nano* **2017**, *11*, 6930.
- [80] X. F. Zhang, J. J. Guo, P. F. Guan, C. J. Liu, H. Huang, F. H. Xue, X. L. Dong, S. J. Pennycook, M. F. Chisholm, *Nat. Commun.* **2013**, *4*, 1924.
- [81] B. Li, X. Zhou, X. Wang, B. Liu, B. Li, *J. Power Sources* **2014**, *272*, 320.
- [82] S. Muralikrishna, T. N. Ravishankar, T. Ramakrishna, D. H. Nagaraju, R. Krishna Pai, *Environ. Prog. Sustainable Energy* **2016**, *35*, 565.
- [83] M. Jahan, Z. L. Liu, K. P. Loh, *Adv. Funct. Mater.* **2013**, *23*, 5363.
- [84] J. Wang, H. Zhang, C. Wang, Y. Zhang, J. Wang, H. Zhao, M. Cheng, A. Li, J. Wang, *Energy Storage Mater.* **2018**, *12*, 1.
- [85] J. Guo, X. Yan, Q. Liu, Q. Li, X. Xu, L. Kang, Z. Cao, G. Chai, J. Chen, Y. Wang, J. Yao, *Nano Energy* **2018**, *46*, 347.
- [86] W. Li, J. Wu, D. C. Higgins, J.-Y. Choi, Z. Chen, *ACS Catal.* **2012**, *2*, 2761.
- [87] H. Yin, C. Z. Zhang, F. Liu, Y. L. Hou, *Adv. Funct. Mater.* **2014**, *24*, 2930.
- [88] Y. G. Li, W. Zhou, H. L. Wang, L. M. Xie, Y. Y. Liang, F. Wei, J. C. Idrobo, S. J. Pennycook, H. J. Dai, *Nat. Nanotechnol.* **2012**, *7*, 394.
- [89] K. Jiang, S. Siahrostami, T. Zheng, Y. Hu, S. Hwang, E. Stavitski, Y. Peng, J. Dynes, M. Gangisetty, D. Su, K. Attenkofer, H. Wang, *Energy Environ. Sci.* **2018**, *11*, 893.
- [90] H. J. Qiu, Y. Ito, W. Cong, Y. Tan, P. Liu, A. Hirata, T. Fujita, Z. Tang, M. Chen, *Angew. Chem., Int. Ed.* **2015**, *54*, 14031.
- [91] H. L. Fei, J. C. Dong, M. J. Arellano-Jimenez, G. L. Ye, N. D. Kim, E. L. G. Samuel, Z. W. Peng, Z. Zhu, F. Qin, J. M. Bao, M. J. Yacaman, P. M. Ajayan, D. L. Chen, J. M. Tour, *Nat. Commun.* **2015**, *6*, 8668.
- [92] H. Zhang, P. An, W. Zhou, B. Y. Guan, P. Zhang, J. Dong, X. W. Lou, *Sci. Adv.* **2018**, *4*, eaao6657.
- [93] J. Wang, Z. Huang, W. Liu, C. Chang, H. Tang, Z. Li, W. Chen, C. Jia, T. Yao, S. Wei, Y. Wu, Y. Li, *J. Am. Chem. Soc.* **2017**, *139*, 17281.
- [94] Y. Han, Y. G. Wang, W. Chen, R. Xu, L. Zheng, J. Zhang, J. Luo, R. A. Shen, Y. Zhu, W. C. Cheong, C. Chen, Q. Peng, D. Wang, Y. Li, *J. Am. Chem. Soc.* **2017**, *139*, 17269.
- [95] H. W. Liang, W. Wei, Z. S. Wu, X. L. Feng, K. Mullen, *J. Am. Chem. Soc.* **2013**, *135*, 16002.
- [96] P. Q. Yin, T. Yao, Y. Wu, L. R. Zheng, Y. Lin, W. Liu, H. X. Ju, J. F. Zhu, X. Hong, Z. X. Deng, G. Zhou, S. Q. Wei, Y. D. Li, *Angew. Chem., Int. Ed.* **2016**, *55*, 10800.
- [97] X. X. Wang, D. A. Cullen, Y. T. Pan, S. Hwang, M. Wang, Z. Feng, J. Wang, M. H. Engelhard, H. Zhang, Y. He, Y. Shao, D. Su, K. L. More, J. S. Spendlow, G. Wu, *Adv. Mater.* **2018**, *30*, 1706758.
- [98] X. Fu, P. Zamani, J. Y. Choi, F. M. Hassan, G. Jiang, D. C. Higgins, Y. Zhang, M. A. Hoque, Z. Chen, *Adv. Mater.* **2017**, *29*, 1604456.
- [99] Y. J. Chen, S. F. Ji, Y. G. Wang, J. C. Dong, W. X. Chen, Z. Li, R. A. Shen, L. R. Zheng, Z. B. Zhuang, D. S. Wang, Y. D. Li, *Angew. Chem., Int. Ed.* **2017**, *56*, 6937.
- [100] Q. Liu, X. Liu, L. Zheng, J. Shui, *Angew. Chem., Int. Ed.* **2018**, *57*, 1218.
- [101] S. Fu, C. Zhu, D. Su, J. Song, S. Yao, S. Feng, M. H. Engelhard, D. Du, Y. Lin, *Small* **2018**, *17*, 1703118.
- [102] Z. Zhang, X. Gao, M. Dou, J. Ji, F. Wang, *Small* **2017**, *13*, 1604290.
- [103] H. Shen, E. Gracia-Espino, J. Ma, H. Tang, X. Mamat, T. Wagberg, G. Hu, S. Guo, *Nano Energy* **2017**, *35*, 9.
- [104] H. T. Chung, D. A. Cullen, D. Higgins, B. T. Sneed, E. F. Holby, K. L. More, P. Zelenay, *Science* **2017**, *357*, 479.
- [105] H. Fei, J. Dong, Y. Feng, C. S. Allen, C. Wan, B. Voloskiy, M. Li, Z. Zhao, Y. Wang, H. Sun, P. An, W. Chen, Z. Guo, C. Lee, D. Chen, I. Shakir, M. Liu, T. Hu, Y. Li, A. I. Kirkland, X. Duan, Y. Huang, *Nat. Catal.* **2018**, *1*, 63.
- [106] H. B. Yang, S.-F. Hung, S. Liu, K. Yuan, S. Miao, L. Zhang, X. Huang, H.-Y. Wang, W. Cai, R. Chen, J. Gao, X. Yang, W. Chen, Y. Huang, H. M. Chen, C. M. Li, T. Zhang, B. Liu, *Nat. Energy* **2018**, *3*, 140.
- [107] L. Fan, P. F. Liu, X. Yan, L. Gu, Z. Z. Yang, H. G. Yang, S. Qiu, X. Yao, *Nat. Commun.* **2016**, *7*, 10667.
- [108] C. Zhao, X. Dai, T. Yao, W. Chen, X. Wang, J. Wang, J. Yang, S. Wei, Y. Wu, Y. Li, *J. Am. Chem. Soc.* **2017**, *139*, 8078.
- [109] G. P. Gao, Y. Jiao, E. R. Waclawik, A. J. Du, *J. Am. Chem. Soc.* **2016**, *138*, 6292.
- [110] Y. Peng, L. Li, R. Tao, L. Tan, M. Qiu, L. Guo, *Nano Res.* **2018**, *11*, 3222.
- [111] Y. Peng, W. Pan, N. Wang, J. E. Lu, S. Chen, *ChemSusChem* **2018**, *11*, 130.
- [112] F. He, K. Li, C. Yin, Y. Wang, H. Tang, Z. Wu, *Carbon* **2017**, *114*, 619.
- [113] Y. Peng, B. Lu, L. Chen, N. Wang, J. E. Lu, Y. Ping, S. Chen, *J. Mater. Chem. A* **2017**, *5*, 18261.
- [114] B. Z. Lu, T. J. Smart, D. D. Qin, J. E. Lu, N. Wang, L. M. Chen, Y. Peng, Y. Ping, S. W. Chen, *Chem. Mater.* **2017**, *29*, 5617.
- [115] Y. Jiao, Y. Zheng, M. T. Jaroniec, S. Z. Qiao, *Chem. Soc. Rev.* **2015**, *44*, 2060.
- [116] J. K. Norskov, T. Bligaard, J. Rossmeisl, C. H. Christensen, *Nat. Chem.* **2009**, *1*, 37.

- [117] S. Kattel, P. Atanassov, B. Kiefer, *Phys. Chem. Chem. Phys.* **2013**, *15*, 148.
- [118] M. Li, S. Wu, X. Yang, J. Hu, L. Peng, L. Bai, Q. Huo, J. Guan, *Appl. Catal., A* **2017**, *543*, 61.
- [119] J. Wang, T. T. Wang, F. B. Wang, D. Y. Zhang, K. Wang, X. H. Xia, *J. Phys. Chem. C* **2016**, *120*, 15593.
- [120] L. Birry, J. H. Zagal, J.-P. Dodelet, *Electrochem. Commun.* **2010**, *12*, 628.
- [121] W. Li, A. Yu, D. C. Higgins, B. G. Llanos, Z. Chen, *J. Am. Chem. Soc.* **2010**, *132*, 17056.
- [122] M. S. Thorum, J. M. Hankett, A. A. Gewirth, *J. Phys. Chem. Lett.* **2011**, *2*, 295.
- [123] J. Wu, W. Li, D. Higgins, Z. Chen, *J. Phys. Chem. C* **2011**, *115*, 18856.
- [124] R. S. Hsu, Z. Chen, *ECS Trans.* **2010**, *28*, 39.
- [125] W. Liu, L. Cao, W. Cheng, Y. Cao, X. Liu, W. Zhang, X. Mou, L. Jin, X. Zheng, W. Che, Q. Liu, T. Yao, S. Wei, *Angew. Chem., Int. Ed. Engl.* **2017**, *56*, 9312.
- [126] X. Zheng, Z. Yang, J. Wu, C. Jin, J.-H. Tian, R. Yang, *RSC Adv.* **2016**, *6*, 64155.
- [127] C. Gao, S. Chen, Y. Wang, J. Wang, X. Zheng, J. Zhu, L. Song, W. Zhang, Y. Xiong, *Adv. Mater.* **2018**, *30*, 1704624.
- [128] Z. P. Chen, S. Pronkin, T. P. Fellingner, K. Kailasam, G. Vile, D. Albani, F. Krumeich, R. Leary, J. Barnard, J. M. Thomas, J. Perez-Ramirez, M. Antonietti, D. Dontsova, *ACS Nano* **2016**, *10*, 3166.
- [129] Z. Liang, C. Qu, D. Xia, R. Zou, Q. Xu, *Angew. Chem.* **2018**, *57*, 9604.
- [130] S. Dang, Q.-L. Zhu, Q. Xu, *Nat. Rev. Mater.* **2017**, *3*, 17075.
- [131] Y. V. Kaneti, J. Tang, R. R. Salunkhe, X. C. Jiang, A. B. Yu, K. C. W. Wu, Y. Yamauchi, *Adv. Mater.* **2017**, *29*, 1604898.
- [132] A. Dhakshinamoorthy, A. M. Asiri, H. García, *Angew. Chem., Int. Ed.* **2016**, *55*, 5414.
- [133] W. Xia, A. Mahmood, R. Zou, Q. Xu, *Energy Environ. Sci.* **2015**, *8*, 1837.
- [134] S. N. Zhao, X. Z. Song, S. Y. Song, H. J. Zhang, *Coordin. Chem. Rev.* **2017**, *337*, 80.
- [135] T. Y. Ma, S. Dai, M. Jaroniec, S. Z. Qiao, *J. Am. Chem. Soc.* **2014**, *136*, 13925.
- [136] X. Zeng, J. Shui, X. Liu, Q. Liu, Y. Li, J. Shang, L. Zheng, R. Yu, *Adv. Energy Mater.* **2018**, *8*, 1701345.
- [137] X. Wang, W. Chen, L. Zhang, T. Yao, W. Liu, Y. Lin, H. Ju, J. Dong, L. Zheng, W. Yan, X. Zheng, Z. Li, X. Wang, J. Yang, D. He, Y. Wang, Z. Deng, Y. Wu, Y. Li, *J. Am. Chem. Soc.* **2017**, *139*, 9419.
- [138] F. Wang, Y. Wang, Y. Feng, Y. Zeng, Z. Xie, Q. Zhang, Y. Su, P. Chen, Y. Liu, K. Yao, W. Lv, G. Liu, *Appl. Catal., B* **2018**, *221*, 510.
- [139] J. K. Gao, J. P. Wang, X. F. Qian, Y. Y. Dong, H. Xu, R. J. Song, C. F. Yan, H. C. Zhu, Q. W. Zhong, G. D. Qian, J. M. Yao, *J. Solid State Chem.* **2015**, *228*, 60.
- [140] Y. Xia, Z. Yang, R. Mokaya, *Nanoscale* **2010**, *2*, 639.
- [141] N. Fechner, T. P. Fellingner, M. Antonietti, *Adv. Mater.* **2013**, *25*, 75.
- [142] B. Liu, H. Shioyama, T. Akita, Q. Xu, *J. Am. Chem. Soc.* **2008**, *130*, 5390.
- [143] J. Yan, Q. Wang, T. Wei, L. Jiang, M. Zhang, X. Jing, Z. Fan, *ACS Nano* **2014**, *8*, 4720.
- [144] P. Strubel, S. Thieme, T. Biemelt, A. Helmer, M. Oschatz, J. Brückner, H. Althues, S. Kaskel, *Adv. Funct. Mater.* **2015**, *25*, 287.
- [145] W. G. Liu, L. L. Zhang, W. S. Yan, X. Y. Liu, X. F. Yang, S. Miao, W. T. Wang, A. Q. Wang, T. Zhang, *Chem. Sci.* **2016**, *7*, 5758.
- [146] W. Liu, L. Zhang, X. Liu, X. Liu, X. Yang, S. Miao, W. Wang, A. Wang, T. Zhang, *J. Am. Chem. Soc.* **2017**, *139*, 10790.
- [147] G. Vile, D. Albani, M. Nachttegaal, Z. Chen, D. Dontsova, M. Antonietti, N. Lopez, J. Perez-Ramirez, *Angew. Chem., Int. Ed.* **2015**, *54*, 11265.
- [148] X. Li, W. Bi, L. Zhang, S. Tao, W. Chu, Q. Zhang, Y. Luo, C. Wu, Y. Xie, *Adv. Mater.* **2016**, *28*, 2427.
- [149] J. Xi, H. Sun, D. Wang, Z. Zhang, X. Duan, J. Xiao, F. Xiao, L. Liu, S. Wang, *Appl. Catal., B* **2018**, *225*, 291.
- [150] V. Georgakilas, J. N. Tiwari, K. C. Kemp, J. A. Permana, A. B. Bourlinos, K. S. Kim, R. Zboril, *Chem. Rev.* **2016**, *116*, 5464.
- [151] S. Canaguier, V. Artero, M. Fontecave, *Dalton Trans.* **2008**, *0*, 315.
- [152] C. Tard, C. J. Pickett, *Chem. Rev.* **2009**, *109*, 2245.
- [153] Y.-T. Kim, K. Ohshima, K. Higashimine, T. Uruga, M. Takata, H. Suematsu, T. Mitani, *Angew. Chem.* **2006**, *118*, 421.
- [154] R. L. Puurunen, *Chem. Vap. Deposition* **2014**, *20*, 332.
- [155] H. Van Bui, F. Grillo, J. R. van Ommen, *Chem. Commun.* **2017**, *53*, 45.
- [156] J. L. Lu, J. W. Elam, P. C. Stair, *Acc. Chem. Res.* **2013**, *46*, 1806.
- [157] S. H. Sun, G. X. Zhang, N. Gauquelin, N. Chen, J. G. Zhou, S. L. Yang, W. F. Chen, X. B. Meng, D. S. Geng, M. N. Banis, R. Y. Li, S. Y. Ye, S. Knights, G. A. Botton, T. K. Sham, X. L. Sun, *Sci. Rep.* **2013**, *3*, 1775.
- [158] X. H. Huang, Y. J. Xia, Y. J. Cao, X. S. Zheng, H. B. Pan, J. F. Zhu, C. Ma, H. W. Wang, J. J. Li, R. You, S. Q. Wei, W. X. Huang, J. L. Lu, *Nano Res.* **2017**, *10*, 1302.
- [159] Z. Li, N. M. Schweitzer, A. B. League, V. Bernales, A. W. Peters, A. Getsoian, T. C. Wang, J. T. Miller, A. Vjunov, J. L. Fulton, J. A. Lercher, C. J. Cramer, L. Gagliardi, J. T. Hupp, O. K. Farha, *J. Am. Chem. Soc.* **2016**, *138*, 1977.
- [160] S. Stambula, N. Gauquelin, M. Bugnet, S. Gorantla, S. Turner, S. H. Sun, J. Liu, G. X. Zhang, X. L. Sun, G. A. Botton, *J. Phys. Chem. C* **2014**, *118*, 3890.
- [161] Z. Cai, B. Liu, X. Zou, H.-M. Cheng, *Chem. Rev.* **2018**, *118*, 6091.
- [162] T. Zhang, L. Fu, *Chem* **2018**, *4*, 671.
- [163] J. Zhao, Q. M. Deng, A. Bachmatiuk, G. Sandeep, A. Popov, J. Eckert, M. H. Rummeli, *Science* **2014**, *343*, 1228.
- [164] I.-Y. Jeon, Y.-R. Shin, G.-J. Sohn, H.-J. Choi, S.-Y. Bae, J. Mahmood, S.-M. Jung, J.-M. Seo, M.-J. Kim, D. W. Chang, *Proc. Natl. Acad. Sci. USA* **2012**, *109*, 5588.
- [165] S. Immohr, M. Felderhoff, C. Weidenthaler, F. Schüth, *Angew. Chem., Int. Ed.* **2013**, *52*, 12688.
- [166] D. H. Deng, X. Q. Chen, L. Yu, X. Wu, Q. F. Liu, Y. Liu, H. X. Yang, H. F. Tian, Y. F. Hu, P. P. Du, R. Si, J. H. Wang, X. J. Cui, H. B. Li, J. P. Xiao, T. Xu, J. Deng, F. Yang, P. N. Duchesne, P. Zhang, J. G. Zhou, L. T. Sun, J. Q. Li, X. L. Pan, X. H. Bao, *Sci. Adv.* **2015**, *1*, e1500462.
- [167] X. J. Cui, J. P. Xiao, Y. H. Wu, P. P. Du, R. Si, H. X. Yang, H. F. Tian, J. Q. Li, W. H. Zhang, D. H. Deng, X. H. Bao, *Angew. Chem., Int. Ed.* **2016**, *55*, 6708.
- [168] A. W. Robertson, C. S. Allen, Y. A. Wu, K. He, J. Olivier, J. Neethling, A. I. Kirkland, J. H. Warner, *Nat. Commun.* **2012**, *3*, 1144.
- [169] A. W. Robertson, B. Montanari, K. He, J. Kim, C. S. Allen, Y. A. Wu, J. Olivier, J. Neethling, N. Harrison, A. I. Kirkland, J. H. Warner, *Nano Lett.* **2013**, *13*, 1468.
- [170] H. Wang, Q. Wang, Y. Cheng, K. Li, Y. Yao, Q. Zhang, C. Dong, P. Wang, U. Schwingenschlogl, W. Yang, X. X. Zhang, *Nano Lett.* **2012**, *12*, 141.
- [171] H. Wang, K. Li, Y. Cheng, Q. Wang, Y. Yao, U. Schwingenschlogl, X. Zhang, W. Yang, *Nanoscale* **2012**, *4*, 2920.
- [172] M. Li, L. Zhang, Q. Xu, J. Niu, Z. Xia, *J. Catal.* **2014**, *314*, 66.
- [173] S. Back, J. Lim, N.-Y. Kim, Y.-H. Kim, Y. Jung, *Chem. Sci.* **2017**, *8*, 1090.
- [174] V. Viswanathan, H. A. Hansen, J. Rossmeisl, J. K. Nørskov, *ACS Catal.* **2012**, *2*, 1654.
- [175] Y. Peng, B. Lu, N. Wang, L. Li, S. Chen, *Phys. Chem. Chem. Phys.* **2017**, *19*, 9336.
- [176] P. Su, K. Iwase, T. Harada, K. Kamiya, S. Nakanishi, *Chem. Sci.* **2018**, *9*, 3941.
- [177] K. Chan, C. Tsai, H. A. Hansen, J. K. Nørskov, *ChemCatChem* **2014**, *6*, 1899.
- [178] A. A. Peterson, J. K. Nørskov, *J. Phys. Chem. Lett.* **2012**, *3*, 251.

- [179] J. Kim, C.-W. Roh, S. K. Sahoo, S. Yang, J. Bae, J. W. Han, H. Lee, *Adv. Energy Mater.* **2018**, *8*, 1701476.
- [180] J. Luo, H. Tang, X. Tian, S. Hou, X. Li, L. Du, S. Liao, *ACS Appl. Mater. Interfaces* **2018**, *10*, 3530.
- [181] S. Yang, Y. J. Tak, J. Kim, A. Soon, H. Lee, *ACS Catal.* **2017**, *7*, 1301.
- [182] R. Q. Zhang, T. H. Lee, B. D. Yu, C. Stampfl, A. Soon, *Phys. Chem. Chem. Phys.* **2012**, *14*, 16552.
- [183] J. Kim, H. E. Kim, H. Lee, *ChemSusChem* **2018**, *11*, 104.
- [184] D. H. Lee, W. J. Lee, W. J. Lee, S. O. Kim, Y. H. Kim, *Phys. Rev. Lett.* **2011**, *106*, 175502.
- [185] F. H. B. Lima, J. Zhang, M. H. Shao, K. Sasaki, M. B. Vukmirovic, E. A. Ticianelli, R. R. Adzic, *J. Phys. Chem. C* **2007**, *111*, 404.
- [186] Y. Wang, H. Yuan, Y. Li, Z. Chen, *Nanoscale* **2015**, *7*, 11633.
- [187] F. Calle-Vallejo, J. I. Martínez, J. Rossmeisl, *Phys. Chem. Chem. Phys.* **2011**, *13*, 15639.
- [188] W. X. Yang, X. J. Liu, X. Y. Yue, J. B. Jia, S. J. Guo, *J. Am. Chem. Soc.* **2015**, *137*, 1436.
- [189] G. Y. Ren, X. Y. Lu, Y. N. Li, Y. Zhu, L. M. Dai, L. Jiang, *ACS Appl. Mater. Interfaces.* **2016**, *8*, 4118.
- [190] J. S. Lee, G. S. Park, S. T. Kim, M. L. Liu, J. Cho, *Angew. Chem., Int. Ed.* **2013**, *52*, 1026.
- [191] W. J. Jiang, L. Gu, L. Li, Y. Zhang, X. Zhang, L. J. Zhang, J. Q. Wang, J. S. Hu, Z. D. Wei, L. J. Wan, *J. Am. Chem. Soc.* **2016**, *138*, 3570.
- [192] C. Walling, *Acc. Chem. Res.* **1975**, *8*, 125.
- [193] S.-F. Kang, H.-M. Chang, *Water Sci. Technol.* **1997**, *36*, 215.
- [194] V. Vij, J. N. Tiwari, W. G. Lee, T. Yoon, K. S. Kim, *Sci. Rep.* **2016**, *6*, 20132.
- [195] C. Mealli, T. B. Rauchfuss, *Angew. Chem., Int. Ed.* **2007**, *46*, 8942.
- [196] Y. Shomura, M. Taketa, H. Nakashima, H. Tai, H. Nakagawa, Y. Ikeda, M. Ishii, Y. Igarashi, H. Nishihara, K. S. Yoon, S. Ogo, S. Hirota, Y. Higuchi, *Science* **2017**, *357*, 928.
- [197] C. Tard, X. M. Liu, S. K. Ibrahim, M. Bruschi, L. De Gioia, S. C. Davies, X. Yang, L. S. Wang, G. Sawers, C. J. Pickett, *Nature* **2005**, *433*, 610.
- [198] A. D. Wilson, R. K. Shoemaker, A. Miedaner, J. T. Muckerman, D. L. DuBois, M. R. DuBois, *Proc. Natl. Acad. Sci. USA* **2007**, *104*, 6951.
- [199] A. Le Goff, V. Artero, B. Josselme, P. D. Tran, N. Guillet, R. Metaye, A. Fihri, S. Palacin, M. Fontecave, *Science* **2009**, *326*, 1384.
- [200] H. Funke, A. C. Scheinost, M. Chukalina, *Phys. Rev. B* **2005**, *71*, 094110.
- [201] T. F. Jaramillo, K. P. Jorgensen, J. Bonde, J. H. Nielsen, S. Horch, I. Chorkendorff, *Science* **2007**, *317*, 100.
- [202] J. Kibsgaard, T. F. Jaramillo, *Angew. Chem., Int. Ed.* **2014**, *53*, 14433.
- [203] J. Kibsgaard, T. F. Jaramillo, F. Besenbacher, *Nat. Chem.* **2014**, *6*, 248.
- [204] J. R. McKone, B. F. Sadtler, C. A. Werlang, N. S. Lewis, H. B. Gray, *ACS Catal.* **2013**, *3*, 166.
- [205] E. J. Popczun, J. R. McKone, C. G. Read, A. J. Biacchi, A. M. Wiltrout, N. S. Lewis, R. E. Schaak, *J. Am. Chem. Soc.* **2013**, *135*, 9267.
- [206] E. J. Popczun, C. G. Read, C. W. Roske, N. S. Lewis, R. E. Schaak, *Angew. Chem., Int. Ed.* **2014**, *53*, 5427.
- [207] J.-M. Yan, Z.-L. Wang, H.-L. Wang, Q. Jiang, *J. Mater. Chem.* **2012**, *22*, 10990.
- [208] J. Ahmed, A. Ganguly, S. Saha, G. Gupta, P. Trinh, A. M. Mugweru, S. E. Lofland, K. V. Ramanujachary, A. K. Ganguli, *J. Phys. Chem. C* **2011**, *115*, 14526.
- [209] B. Kumar, S. Saha, M. Basu, A. K. Ganguli, *J. Mater. Chem. A* **2013**, *1*, 4728.
- [210] W. Chen, J. Pei, C. T. He, J. Wan, H. Ren, Y. Zhu, Y. Wang, J. Dong, S. Tian, W. C. Cheong, S. Lu, L. Zheng, X. Zheng, W. Yan, Z. Zhuang, C. Chen, Q. Peng, D. Wang, Y. Li, *Angew. Chem., Int. Ed.* **2017**, *56*, 16086.
- [211] J. Zhang, X. Chen, K. Takanabe, K. Maeda, K. Domen, J. D. Epping, X. Fu, M. Antonietti, X. Wang, *Angew. Chem., Int. Ed. Engl* **2010**, *49*, 441.
- [212] B. Wurster, D. Grumelli, D. Hotger, R. Gutzler, K. Kern, *J. Am. Chem. Soc.* **2016**, *138*, 3623.
- [213] J. Zhang, Z. Zhao, Z. Xia, L. Dai, *Nat. Nanotechnol.* **2015**, *10*, 444.
- [214] P. Liao, J. A. Keith, E. A. Carter, *J. Am. Chem. Soc.* **2012**, *134*, 13296.
- [215] K. Xu, H. Ding, H. Lv, P. Chen, X. Lu, H. Cheng, T. Zhou, S. Liu, X. Wu, C. Wu, *Adv. Mater.* **2016**, *28*, 3326.
- [216] C. C. McCrory, S. Jung, J. C. Peters, T. F. Jaramillo, *J. Am. Chem. Soc.* **2013**, *135*, 16977.
- [217] K. Fan, H. Chen, Y. Ji, H. Huang, P. M. Claesson, Q. Daniel, B. Philippe, H. Rensmo, F. Li, Y. Luo, *Nat. Commun.* **2016**, *7*, 11981.
- [218] J. Ren, M. Antonietti, T. P. Fellingner, *Adv. Energy Mater.* **2015**, *5*, 1401660.
- [219] X. Zhang, Z. Wu, X. Zhang, L. Li, Y. Li, H. Xu, X. Li, X. Yu, Z. Zhang, Y. Liang, H. Wang, *Nat. Commun.* **2017**, *8*, 14675.
- [220] Y. Liang, Y. Li, H. Wang, H. Dai, *J. Am. Chem. Soc.* **2013**, *135*, 2013.
- [221] N. Morlanés, K. Takanabe, V. Rodionov, *ACS Catal.* **2016**, *6*, 3092.
- [222] S. Lin, C. S. Diercks, Y. B. Zhang, N. Kornienko, E. M. Nichols, Y. Zhao, A. R. Paris, D. Kim, P. Yang, O. M. Yaghi, C. J. Chang, *Science* **2015**, *349*, 1208.
- [223] C. Costentin, M. Robert, J. M. Saveant, *Acc. Chem. Res.* **2015**, *48*, 2996.
- [224] G. Gao, S. Bottle, A. Du, *Catal. Sci. Technol.* **2018**, *8*, 996.
- [225] D. Friebel, M. W. Louie, M. Bajdich, K. E. Sanwald, Y. Cai, A. M. Wise, M.-J. Cheng, D. Sokaras, T.-C. Weng, R. Alonso-Mori, *J. Am. Chem. Soc.* **2015**, *137*, 1305.
- [226] M. Ledendecker, G. Clavel, M. Antonietti, M. Shalom, *Adv. Funct. Mater.* **2015**, *25*, 393.
- [227] R. Subbaraman, D. Tripkovic, D. Strmcnik, K.-C. Chang, M. Uchimura, A. P. Paulikas, V. Stamenkovic, N. M. Markovic, *Science* **2011**, *334*, 1256.
- [228] Z. L. Wang, D. Xu, J. J. Xu, X. B. Zhang, *Chem. Soc. Rev.* **2014**, *43*, 7746.
- [229] D. U. Lee, P. Xu, Z. P. Cano, A. G. Kashkooli, M. G. Park, Z. Chen, *J. Mater. Chem. A* **2016**, *4*, 7107.
- [230] S. Zhao, L. Yan, H. Luo, W. Mustain, H. Xu, *Nano Energy* **2018**, *47*, 172.
- [231] P. Chen, T. Zhou, L. Xing, K. Xu, Y. Tong, H. Xie, L. Zhang, W. Yan, W. Chu, C. Wu, Y. Xie, *Angew. Chem., Int. Ed.* **2017**, *56*, 610.
- [232] A. Aijaz, J. Masa, C. Rösler, W. Xia, P. Weide, A. J. R. Botz, R. A. Fischer, W. Schuhmann, M. Muhler, *Angew. Chem., Int. Ed.* **2016**, *55*, 4087.
- [233] N. Ranjbar Sahraie, J. P. Paraknowitsch, C. Gobel, A. Thomas, P. Strasser, *J. Am. Chem. Soc.* **2014**, *136*, 14486.
- [234] J. Wang, H. Wu, D. Gao, S. Miao, G. Wang, X. Bao, *Nano Energy* **2015**, *13*, 387.
- [235] P. G. Hu, L. M. Chen, X. W. Kang, S. W. Chen, *Acc. Chem. Res.* **2016**, *49*, 2251.